Neural correlates of minimal recognizable configurations in the human brain

Antonino Casile[1+], Aurelie Cordier[2+], Jiye G. Kim[2], Andrea Cometa[3], Joseph R. Madsen[2], Scellig Stone[2], Guy Ben-Yosef[4], Shimon Ullman[4,6], William Anderson[5], Gabriel Kreiman[2,6,*]

[1] Department of Biomedical and Dental Sciences and Morphofunctional Imaging University of Messina 98124 Messina (ME), Italy
[2] Children's Hospital, Harvard Medical School, Boston, MA 02115, USA
[3]MoMiLab, IMT School for Advanced Studies, 55100 Lucca (LU), Italy
[4] Weizmann Institute, Rehovot, Israel
[5] Department of Neurosurgery, Johns Hopkins Medical School, Baltimore 21205, MD, USA
[6] Center for Brains, Minds and Machines, Cambridge, MA 02142, USA

[+] Equal contribution
[*] To whom correspondence should be addressed: Gabriel.kreiman@tch.harvard.edu

Summary

Inferring object identity from incomplete information is a ubiquitous challenge for the visual system. Here we study the neural mechanisms underlying processing of minimally recognizable configurations (MIRCs) and their subparts which are unrecognizable (sub-MIRCs). MIRCs and sub-MIRCs are very similar at the pixel level, yet they lead to a dramatic gap in recognition performance. To evaluate how the brain processes such images, we invasively record human neurophysiological responses. Correct identification of MIRCs is associated with a dynamic interplay of feedback and feedforward mechanisms between frontal and temporal areas. Interpretation of sub-MIRC images improves dramatically after exposure to the corresponding full objects. This rapid and unsupervised learning is accompanied by changes in neural responses in the temporal cortex. These results are at odds with purely feedforward models of object recognition and suggest a role for the frontal lobe in providing top-down signals related to object identity in difficult visual tasks.

[*] Lead contact

Introduction

Visual object recognition is robust to an extensive range of image transformations that produce different retinal projections of the same stimulus [1,2]. For example, we can easily recognize an object when presented under a wide range of positions, scales, or viewpoints [3,4]. A particularly striking example of the robustness of visual perception is the ability to recognize an object when only a fragment of it is shown. Fragmented object views are ubiquitous during natural vision due to occlusion or poor illumination. In these cases, the visual representation of the objects is incomplete, and yet our visual system can quickly, and seemingly effortlessly, compensate for the missing information [5–11].

It has been proposed that objects in the visual scene have features that can be reliably extracted across a wide variety of viewing conditions and which support perception [2,12–15]. Several experimental methods that allow the identification of such informative features have been proposed. For example, Gosselin & Schyns (2001) proposed a technique called Bubbles that consisted in presenting objects through apertures to identify specific "critical features" that can aid recognition [17–19] and are represented in neural signals [20,21]. Other studies have used images with different levels of fragmentation or occlusion [10,22] to investigate frequency bands or time points of the event-related potentials that are enhanced during recognition [23–25].

Recently, Ullman and colleagues extended the notion of critical features in a study that combined large-scale human psychophysical experiments and computer vision [26]. By sequentially cropping and blurring images of objects and assessing their recognition rates, the authors identified MInimally-Recognizable Configurations (MIRCs). MIRCs consist of image fragments recognized by human participants but rendered unrecognizable upon the introduction of minimal changes (**Figure 1**). Small reductions of a MIRC image along the horizontal and vertical dimensions lead to a sub-MIRC image with recognition rates that drop by many tens of percentage points [26]. This dramatic drop in recognition performance from MIRCs to sub-MIRCs cannot be accounted for by state-of-the-art computer vision models [26] and highlights a critical difference between biological vision and current computational models of vision [27].

Occlusion removes large parts of an object from view, but often has a limited impact on perceptual recognition. In contrast, MIRC and sub-MIRC images are very similar in pixel space, but they produce dramatically different recognition performance. Thus, MIRC images offer a unique opportunity to probe visual recognition processes in the presence of stimuli that are very similar at the retinal level while eliciting dramatic differences at the perceptual level [28]. To understand the neural mechanisms that lead to recognition of objects from fragments, we set out to investigate the neurophysiological responses in the human brain

while participants identified MIRC and sub-MIRC images. We recorded invasive neurophysiological responses from patients with epilepsy implanted with electrodes for clinical purposes and investigated the neural correlates of object recognition by comparing neural responses recorded during recognized MIRCs vs. unrecognized sub-MIRCs images. Furthermore, participants rapidly learned to recognize sub-MIRC images after exposure to the full object images. Such learning was accompanied by neural changes that distinguished between identical images when they were recognized versus when they were not recognized.

Results

We recorded intracranial field potentials (IFPs) from 1,752 electrodes (**Table S1**, **Figures S1 and S7**) in 12 participants (5 male, 11–43 years old, **Table S2**) implanted with subdural or deep intracerebral electrodes to localize their epileptic seizure foci. Participants viewed grayscale images for 1s and were then asked to identify them verbally (**Figure 1A**). Participants were given no feedback about the correctness of their responses.

Participants rapidly learned to recognize images in an unsupervised fashion

Visual stimuli were a subset of the images used by Ullman and colleagues in a previous large-scale behavioral study [26]. The stimuli included images from 10 object categories (**Figure 1B**) or degraded versions of those images obtained by iteratively cropping or changing the resolution of the original image [26]. In the original study, Ullman and colleagues tested stimuli at many different levels of degradation and observed that there were critical levels of degradation that led to a sharp drop in performance. They operationally defined MIRCs as image patches that could be reliably recognized on average by human observers and for which further reduction in either size or resolution made the patch unrecognizable. A non-recognizable descendant of a MIRC image was called a sub-MIRC (**Figure 1C**).

In our experiments, we presented image patches at different levels of degradation. To minimize potential adaptation effects, stimuli were presented in a mini-block design paradigm. Within each mini-block, images from two out of the ten categories were presented starting from the most degraded stimuli (sub-MIRCs, red in **Figure 1C**), followed by MIRCs (blue in **Figure 1C**), and then the original (undegraded) images (object, black in **Figure 1C**). The same sub-MIRC stimuli were shown again at the end of each mini-block (sub-MIRC post, dashed red in **Figure 1C**). Each participant completed 5 consecutive mini-blocks so as to present stimuli from all 10 categories. The order of presentation of the categories was randomized across participants.

Figure 1D shows recognition performance across our pool of 12 participants. Consistent with the experimental results in Ullman et al.'s study and with the definition above, there was a large drop in performance between MIRCs and sub-MIRCs ($p<<0.01$, paired t-test). Notably, this drop was sharp and similar to that measured in the general population (71% drop in the general population [26], 87% drop in **Figure 1D**). Furthermore, here we observed a substantial increase in performance between the initial and the final sub-MIRC blocks ("sub-MIRC" and "sub-MIRC post" conditions in **Figure 1D**, 78% increase, $p<<0.01$, paired t-test). That is, the same images that were unrecognizable in the first block (sub-MIRC condition) became recognizable, almost on par with the MIRC images themselves, after exposure to the MIRC and object images (sub-MIRC post condition). This result demonstrates a rapid increase in recognition rates of the sub-MIRC images after presentation of MIRC and object images in the previous blocks. Taken together, the results of **Figure 1D** suggest that our pool of patients, although necessarily smaller than the original large cohort reported in Ullman et al.'s study, showed behavior concordant with that of the general population. In addition, these results demonstrate a rapid and substantial increase in the recognition of sub-MIRC images, after exposure to their associated MIRC and undegraded versions.

Minimal image changes between MIRCs and sub-MIRCs elicited large differences in neural responses

To investigate the neural representation of MIRC and sub-MIRC stimuli, we implemented several changes in the experimental paradigm compared to the original work by Ullman and colleagues [26] (**Methods**): (i) while the original study was based on across-participant averages, here we focus on within-participant comparisons; (ii) because of the within-participant design, we first determined the perceptual threshold between MIRC and sub-MIRC stimuli separately for each image and participant; (iii) to assess the reliability of neural responses, each stimulus was repeated 10 times, (iv) to ensure that we could reliably measure neural responses to sub-MIRCs without any learning, the sub-MIRC stimuli were presented before the MIRC stimuli.

We first investigated the neural correlates of the perceptual differences between the recognized MIRC and the unrecognized sub-MIRC stimuli. An electrode was considered to be visually selective if it was responsive to either MIRC or sub-MIRC stimuli and the intracranial field potentials (IFPs) elicited by the MIRC images were significantly different from those elicited by the sub-MIRC stimuli for at least 50 consecutive ms in the interval [50,550]ms after stimulus onset (see **Methods**).

Figure 2 shows a representative electrode located in the left inferior frontal cortex (**Figure 2A**). Consistent with previous neurophysiological recordings [29], this electrode showed strong evoked responses

shortly after presentation of the visual stimuli. These responses were stronger for MIRC (blue) and object (black) stimuli, as shown by the large change in IFPs after stimulus onset with respect to the preceding baseline (see average responses in **Figure 2B** and raster plots showing responses in individual trials in **Figure 2C**). Furthermore, the neural responses were significantly different for MIRCs versus sub-MIRCs in the time interval marked by the black horizontal line (**Figure 2D**) and for object vs sub-MIRC in a similar interval (**Figure 2B**). We also observed a trend toward a difference between sub-MIRC post vs. sub-MIRC stimuli that did not pass our strict statistical criteria (**Figure 2E**). It is important to emphasize that, at the pixel level, the difference between the MIRC and sub-MIRC stimuli is minimal (**Figure 1C**). Yet, the two stimuli led to considerable differences both at the behavioral (**Figure 1D**) and neural (**Figure 2D**) levels. Across the entire dataset, we observed electrodes that distinguished MIRCs and sub-MIRC images, like the example in **Figure 2,** over an extended network mostly encompassing the temporal (n=48, 20% of responsive electrodes in that area) and frontal (n=58, 29% of responsive electrodes) cortices (**Figure 3A**). A small number of selective electrodes were also found in the occipital (n=11, 10% of responsive electrodes) and parietal (n=9, 9% of responsive electrodes) cortices.

We next evaluated the time at which differential responses between MIRCs and sub-MIRCs emerged. The median time of emergence of selective responses for MIRC versus sub-MIRC stimuli was shorter in the temporal lobe (median=343ms) compared to the frontal lobe (median=368ms), with no statistically significant difference between the two areas (**Figure 3B**, Mann-Whitney U-test=1599, p=0.19, **Methods**). Examination of onset times for responses selective to MIRCs compared to sub-MIRCs in frontal areas revealed that they were not unimodally distributed (Hartingan's dip test = 0.1, p=0.0002 [30]). Indeed, the distribution of the times when selectivity started across different electrodes revealed two components: a first "early" component with onset times smaller than 420ms (n=34 electrodes, median=329ms) and a second "late" component with onset times greater than 420ms (n=24 electrodes, median=478ms; **Figure S6**). Interestingly, the median onset time of early responses in frontal regions (median=329ms) was significantly shorter than the median onset time in temporal regions (Mann-Whitney U-test=580, p=0.021), which, in turn, was shorter than the median onset time of late frontal responses (Mann-Whitney U-test=1029, $p=6.4\cdot10^{-8}$). Due to limited electrode sampling, this bimodality could only be verified in a single participant when examining the onset of selective responses at the individual participant level.

These results suggest that during recognition of MIRC stimuli the emergence of selective responses in frontal areas can precede that in temporal areas. To further investigate this point, we used functional interaction analysis to evaluate the temporal dynamics of the activation of temporal and frontal areas during recognition of MIRC stimuli. To have sufficient statical power, we focused on the participants that had more than one responsive electrode in both the temporal and frontal lobes (n=6 participants) and we used

generalized Partial Directed Coherence (gPDC, [31,32]) to assess the information flow between the frontal and temporal lobes. gDPC provides a measurement of the directed linear relationship between pairs of time series, allowing to quantitatively compare the strength, directionality, and statistical significance of interactions between areas (see **Methods**). The two curves in **Figure 4A** show the average of the gDPC across subjects and pairs of frontal and temporal electrodes (n=3,639 electrode pairs), and thus of the information flow, in the frontal to temporal (green curve) and temporal to frontal (blue curve) directions, respectively, with red shaded areas signifying time intervals when the two curves are significantly different ($p<0.05$ based on a bootstrapping analysis, see **Methods**). In the time interval immediately following the presentation of MIRC stimuli, gPDC was significantly stronger in the top-down fronto-temporal direction (red shaded areas in **Figure 4A**). This prevalence of a top-down fronto-temporal directionality disappeared shortly after 300ms after MIRC presentation, and, after that time, the flow of information was either significantly stronger in the opposite bottom-up temporo-frontal direction or equally strong in the two directions (**Figure 4A**). Next, we computed, for each frontal electrode, the time at which the functional interactions to and from all paired temporal electrodes was significantly stronger in either the frontal-temporal or temporal-frontal direction. As shown by the two distributions in **Figure 4B**, the median onset time at which the interactions were significantly stronger in the frontal to temporal direction was significantly earlier than when it was stronger in the temporal to frontal direction (median frontal→temporal=96ms, median temporal→frontal=312ms; Mann-Whitney U-test=675, p=0.028).

Neural changes accompanied learning to recognize sub-MIRC images

Participants could not recognize sub-MIRC stimuli when presented in the first part of each mini-block. However, these same stimuli became recognizable after exposure to the MIRC and object images (**Figure 1D**). We next asked how this rapid increase in recognition performance was reflected in the neural signals by comparing the IFP responses to sub-MIRC post versus sub-MIRC stimuli.

The example electrode in **Figure 2** showed a significant difference between the responses to MIRCs versus sub-MIRCs (**Figure 2D**) and a trend toward a difference between the sub-MIRCs post versus sub-MIRCs which did not reach statistical significance (**Figure 2E**). The example electrode in **Figure 5**, located in the in the inferior temporal cortex (Figure 5A), exhibited strong evoked responses during the presentation of MIRC (blue) and also during presentation of sub-MIRC post (dashed red) stimuli (**Figure 5B**). Similar to the electrode in Figure 2, the electrode in Figure 5 distinguished MIRC from sub-MIRC stimuli (**Figure 5D**). In contrast to the example electrode in Figure 2, the electrode in Figure 5 also exhibited a significantly different response to sub-MIRC post vs. sub-MIRC images (**Figure 5E**). These differences were also evident in single trials (**Figure 5C**). Notably, sub-MIRC post and sub-MIRC stimuli are identical.

Thus, this difference in neural responsiveness reflects the rapid and unsupervised learning processes that made sub-MIRC post stimuli recognizable.

A comparison of the neural responses to sub-MIRC post versus sub-MIRC stimuli across all electrodes revealed selective responses reflecting recognition primarily for electrodes located in the temporal lobe (n=17, 9% of responsive electrodes in that area). A small number of selective electrodes was also found in occipital (n=6, 6% of responsive electrodes in that area), parietal (n=6, 10% of responsive electrodes in that area) and frontal (n=5, 5% of responsive electrodes in that area) lobes (**Figure 6A**). The median onset times of selective responses to sub-MIRC post versus sub-MIRC stimuli in the temporal lobe was 252ms (**Figure 6B**).

Discussion

We recorded neurophysiological responses from the human brain during recognition of MInimally Recognizable Configuration (MIRC) images and sub-MIRCs [26]. MIRCs and sub-MIRCs exhibit small differences at the pixel level. Yet, the participants showed a dramatic perceptual transition, recognizing MIRCs while failing to recognize sub-MIRCs (**Figure 1D**). After exposure to the MIRC and object stimuli, participants could recognize the same sub-MIRC images that they could not recognize initially (**Figure 1D**). These behavioral observations were accompanied by temporally- and spatially-specific neural responses. Selective responses to MIRCs emerged in frontal and temporal cortex and the interactions between these two areas switched from an earlier frontal to temporal direction to a later temporal to frontal direction (**Figures 3**, **4**). Furthermore, the rapid increase in recognition of sub-MIRCs was associated with the emergence of selective responses predominantly in the temporal lobe (**Figures 5, 6**).

In our experiments, the frontal lobe appeared to have an important role in the recognition of MIRC stimuli. A role of this brain region in the perception, recognition and categorization of objects [33] is supported by experiments in monkey showing that frontal cortex contains neurons selective for complex visual stimuli [33–40]. In particular, frontal areas seem to be specifically involved in the processing of challenging stimuli, such as ambiguous, occluded or masked objects [23,24,41–43]. For instance, monkey prefrontal cortex neurons are more activated by occluded objects that are hard to identify [44] and inactivation of ventral pre-frontal cortex impairs encoding and recognition of challenging images [45,46]. Furthermore, frontal areas seem to have a role in the learning and retrieval of perceptual categories [47–52]. MIRC images are, by definition, challenging to recognize as they contain only minimal information about the depicted object and their recognition entails long integration times[53]. In line with that, **Figures 3** and **4** suggest that recognition of MIRC stimuli is associated with an initial top-down functional interaction from the frontal to the temporal

lobe followed by a later bottom-up interaction in the opposite direction. This result is corroborated by a frequency-resolved gDPC analysis showing that, in agreement with recent proposals [54–57], the initial frontal to temporal flow of information is carried by lower temporal frequencies in the beta range, while the later temporal to frontal flow of information is mainly carried out by higher temporal frequencies in the gamma range (**Figure S8**). Interestingly, a functional interaction analysis on the sub-MIRC trials revealed only a feedforward flow of information from temporal to frontal areas (**Figure S3**). This result might seem at odds with the intuition that the unrecognized sub-MIRC stimuli could produce "hypotheses" in the frontal cortex that are fed back to temporal areas without reaching confirmation. However, the functional interactions analysis reveals directed interactions between neural responses in frontal and temporal areas. In the case of sub-MIRCs, there is a feedforward interaction between temporal and frontal responses that is related to visual processing of these stimuli. The opposite frontal to temporal interactions are missing, perhaps because any activity in frontal areas related to "hypotheses formulation" did not produce a corresponding recognition-related activity in temporal areas given that sub-MIRC stimuli were, by definition, not recognized.

The frontal lobe is also implicated in speech production [58]. It might be thus hypothesized that the selective responses that we observed in frontal areas might be, at least partially, due to the preparatory activity related to the task of verbally reporting their percept that the participants had to carry out. Two reasons make this interpretation of our results unlikely. First, our participants had to verbally report their percept in all conditions. The results of **Figure 3** were obtained by contrasting IFPs produced by MIRC stimuli with those produced by sub-MIRC stimuli and this contrast should thus discount potential neuronal activations related to speech preparation that are common to the two conditions. Second, the contrast sub-MIRC post vs sub-MIRC (**Figure 6**) produced virtually no selective responses in frontal areas. Participants had to verbally report their percept also in these two conditions and the recognition rates of sub-MIRC post stimuli were also comparable to those of MIRC stimuli (**Figure 1D**), that produced instead widespread selective responses in the frontal lobe (**Figure 3**).

Perception of MIRC stimuli elicited widespread activations also in the temporal lobe (**Figure 3**). This brain region has also been implicated in the recognition of occluded and ambiguous stimuli. Indeed, studies have shown signals in the human inferior temporal cortex that may reflect the processing of occluded stimuli [20,23,24,59–61]. In the same vein, studies in monkeys have identified populations of neurons in infero-temporal cortex whose responses correlated with the spatial extent of the occluder or that declined with the degree of occlusion of a to-be-recognized shape [44,62–64]. The selective responses for MIRCs that we found in the temporal lobe might thus also reflect the activation of neural processes involved in their recognition. This proposal is also consistent with a neuroimaging study in humans that showed, in agreement with results

reported here, that the MIRCs vs sub-MIRCs contrast generated extensive activations in several regions of the temporal lobe [65]. Taken together, the pattern of activations during the perception of MIRC stimuli suggests that their recognition might rely on the dynamic interplay of fronto-temporal neural processes.

Participants quickly learned to recognize sub-MIRC images after being exposed, in previous blocks and with no feedback, to the associated MIRC and object images (**Figure 1D**). This striking difference in recognition performance was correlated with concomitant changes in the neural responses, predominantly in the temporal lobe (**Figures 5,6**). Because the sub-MIRC post stimuli are, by definition, identical to the sub-MIRC stimuli presented initially, these neural responses reflect the participant's distinct perceptual experience between the initial and subsequent encounters with these complex stimuli. The results are reminiscent of a very interesting study by Tovee et al. [66] in which they found a change in the responses of single units in the macaque temporal lobe during the observation of degraded visual stimuli before and after exposure to their undegraded and fully recognizable versions.

Consistent with the fact that MIRC and sub-MIRC images are very similar at the pixel level [26], their contrast produced a low number of selective responses in low-level areas in the occipital lobe (n=11, **Figure 3**). In agreement with this observation, an even lower number of selective responses in occipital cortex was produced by the contrast sub-MIRC post vs sub-MIRC (n=6, **Figure 6**), where the presented stimuli were indeed the same in both conditions. These results are in agreement with the notion that the occipital lobe is mainly involved in the processing of low-level characteristics of visual stimuli [67] and further strengthen the conclusion that recognition of MIRC stimuli relies on high-level, rather than low-level, mechanisms.

For both MIRC and sub-MIRC post stimuli, the median time at which selective neural signals emerged in the temporal lobe was around 250-350ms (**Figures 3 and 6**), which is longer than the typical latencies of 100-200ms reported for the decoding of object identity from population responses [29,68,69]. At the behavioral level, MIRC stimuli are known to produce long response times which might be the result of long integration processes [53,70]. Here, we specifically focused on these recognition processes by comparing IFPs elicited by recognized stimuli (MIRC or sub-MIRC post) versus those elicited by the unrecognized sub-MIRC stimuli in the interval from 50 to 550ms after stimulus onset. In contrast, many earlier studies focused on the neural responses to easy-to-recognize stimuli [69] in a shorter temporal window (e.g. [50, 300]ms [29,68] after stimulus onset. Thus, the longer median onset time that we found may be related to the accumulation of evidence that is needed to recognize the challenging MIRC stimuli and the relatively long search interval that we considered. In line with this interpretation, long latencies, similar to those reported here, have been reported in previous human studies that investigated perceptual closure processes by contrasting, similar to our approach, challenging-to-recognize stimuli versus unrecognized stimuli [20,59,60,71]

or the timing of conscious perception [72–75] in a large temporal window after stimulus onset. Indeed, as shown in **Figure S4**, visual responses to MIRC stimuli (i.e. MIRC responses significantly different from baseline) in the [50, 350]ms interval exhibited a sensibly shorter median latencies (median =152ms and 208ms in the occipital and temporal lobe respectively, **Figure S4A**) that are in line with previous decoding studies, with several of these responses starting already before 100ms (**Figure S4B**).

Limitations of the study

In Ullman *et al*.'s original study on minimally recognizable configurations, each participant was exposed to a single stimulus for each category and was never tested again; thus, all the comparisons were between participants [26]. Our study focused on the neural responses to such stimuli and therefore several changes were introduced with respect to the original experimental design. Our study focuses on comparisons within participants, which required presenting different levels of degradation of the original images in sequential order: as shown in **Figure 1D**, participants recognize sub-MIRC images after exposure to the MIRC and object images. To ensure reproducibility, stimuli are repeated multiple times in contrast to the single presentations in Ullman *et al*'s original work (**Methods**).

All the neural data in our study come from patients with pharmacologically-resistant epilepsy. As a consequence, the number and location of electrodes are dictated solely by clinical criteria. Although we had extensive coverage of brain locations (**Table S1**, **Figure S1 and S7**), this sampling was necessarily not exhaustive. Thus, other regions, not sampled here, may also contribute to processing MIRC, sub-MIRC, and sub-MIRC post stimuli.

The age range in our study is limited by the availability of patients with pharmacologically-resistant epilepsy. Previous developmental studies show that, by the age of 11, visual object perception has several adult-like behavioral characteristics [76,77]. Additionally, the behavioral results in Figure 1D are consistent with previous work [26]. However, it is possible that a much larger sample of patients at different ages could help better delimit the development of interactions between ventral visual cortex and frontal cortex regions during recognition of complex images.

Conclusions

There has been exciting progress in developing computational models that provide a first-order approximation to the cascade of computations along the ventral visual cortex during object recognition [78–81]. These models can capture aspects of visual recognition behavior in monkeys and humans [82] and can also approximate neural responses along the ventral visual cortex [83]. Despite these successes, multiple pieces of evidence have highlighted that these models fail to account for the whole repertoire of visual behavior and neurophysiology [84,85]. In particular, these models fail to account for recognition of MIRC stimuli [26].

Challenging stimuli like MIRCs, and especially the sharp transition from sub-MIRC to MIRC in the neural and behavioral responses, provide important constraints to develop future models that incorporate recurrent computations hypothesized to be critical for recognition.

Resource availability

Lead contact. Gabriel Kreiman (Gabriel.kreiman@tch.harvard.edu)

Materials availability. This study did not use or generate any reagents.

Data and code availability. All the data and code are publicly available through the following website: https://kreimanlab.com/code/mirc/

Acknowledgments. We thank all the patients for participating in these experiments. This work was supported by BSH-NSF Grant 1746365 (SU and GK), NIH grant R01EY026025 (GK), by the Center for Brains, Minds and Machines (SU and GK).

Author contributions. The experiments were designed by SU, GBY, JGK, and GK. SS and JRM performed the surgeries. JGK collected the data. Data analyses were performed by AC, AuC and JGK. The manuscript was written by AC, AuC and GK, with feedback and approval from all the authors.

Declaration of interest. The authors have no conflicts of interest to disclose.

Figure legends

Figure 1 – Experimental design and behavioral performance*. (**A**) Temporal unfolding of each trial. A trial started either 3 seconds after the end of the previous trial or upon a key press from the participant. A fixation cross was first shown for 400 ms, followed by an image shown for 1 second. After the image disappeared, the participant was asked to verbally identify the image. (**B**) The 10 images of objects or objects parts used as base stimuli. (**C**) Temporal order of the conditions presented in the experiments. MIRC (MInimal Recognizable Configurations, blue) and sub-MIRC (red) stimuli were images obtained by cropping or changing the resolution of the base images. MIRC images were defined as image patches that are reliably recognized by observers and for which further reduction in either size or resolution makes the patch unrecognizable. A non-recognizable descendant of a MIRC image was called a sub-MIRC [26]. Object (black) stimuli were a subset of the base images in **B**. The sub-MIRCs post (dashed red) stimuli consisted of the same sub-MIRCs images from block 1, presented again at the end of the experiment, after participants were exposed to the MIRC and object images. (**D**) Recognition performance (fraction correct) for each stimulus condition (n=12 participants). Notice the sharp drop in performance between MIRC (blue) and sub-MIRC (red) images and the increased performance in the sub-MIRC post (red stripes) compared to the sub-MIRC images. Error bars represent standard error of the mean.*

Figure 2 – Neural responses distinguished MIRCs from sub-MIRC images*. (**A**) Example electrode in the triangular part of the left inferior frontal gyrus shown on a template brain (MNI coordinates = [-53.4, 27.9, 11]). (**B**) Neural responses of the example electrode in the four experimental conditions (**Fig. 1C**): object (black), MIRC (blue), sub-MIRC (red) and sub-MIRC post (dashed red). The curves represent the mean intracranial field potential (IFP) response in each condition, aligned to stimulus onset (t=0, vertical black dashed line) and averaged across all trials. The shaded area around each curve indicates standard error of the mean. The number of trials in the different conditions are shown in the legend at the bottom. The gray rectangle marks the interval considered for the analysis of neural responses. (**C**) Same responses as in panel **B**, showing all individual trials as raster plots (see scale bar in color map on the right). The color of each box's border indicates the experimental condition. (**D, E**) Responses to MIRC and sub-MIRC stimuli (**D**), and sub-MIRC post and sub-MIRC stimuli (**E**). The black horizontal line in **D** shows the interval in which responses to MIRCs and sub-MIRCs were statistically different ($p<0.01$, Mann-Whitney U-test).*

Figure 3 - Selective responses to MIRCs vs sub-MIRCs exhibited spatial and temporal specificity. *(**A**) Locations of electrodes exhibiting significantly different responses between MIRCs and sub-MIRCs (n=156). Selective responses were mostly located in the temporal (n=48) and frontal (n=58) cortex. Each circle represents an electrode; the color codes the time at which an electrode started to differentiate between MIRCs and sub-MIRCs. (**B**) Distribution of selectivity start times for the MIRC vs. sub-MIRC comparison in the frontal and temporal lobes (median temporal lobe=343ms; median frontal lobe=368ms). The distributions of onset times for electrodes located in the occipital and parietal cortex were not plotted here since only n=11 and n=9 electrodes, respectively, were found. The brain locations of the remaining n=30 electrodes could not be determined.*

Figure 4 – Temporal dynamics of the functional interactions between temporal and frontal areas during the perception of MIRC stimuli. *(**A**) Strength, as assessed by generalized Partial Directed Coherence (gDPC [31]), of the temporal to frontal (blue curve) and frontal to temporal (green curve) functional interactions measured in participants (n=6) that had at least 2 responsive electrodes in <u>both</u> the temporal and frontal*

lobe. The curves represent the average gPDC obtained from n=3639 pairs of frontal and temporal electrodes respectively. Standard errors are shown but they are too small to be visible. Red-shaded areas mark intervals where the interactions in one direction are significantly stronger than in the opposite direction. The functional interactions are initially stronger in the frontal to temporal direction and they subsequently (after approximately 400ms) become either equally strong in the two directions or stronger in the temporal to frontal direction. ***(B)*** *Distributions, across all examined frontal electrodes, of the onset times at which the functional interactions were stronger in the frontal to temporal compared to the opposite temporal to frontal direction (green) or the other way around (blue). The medians of the two distributions were significantly different (Mann-Whitney U-test=675, p=0.028. Frontal → temporal: median = 96ms; Temporal → frontal: median = 312ms).*

Figure 5 *–* ***Selective responses to sub-MIRC post versus sub-MIRC images.*** *Example electrode in the left inferior temporal cortex (MNI coordinates = [-32.7, -27.1, -23.6]). The layout of the panels and symbols follow the format in* ***Figure 2****. This electrode showed a significantly different response between sub-MIRC post (dashed red) and sub-MIRC (red) (****E****) and between MIRC (blue) and sub-MIRC (red) (****D****).*

Figure 6 – Sub-MIRCs post stimuli elicited selective responses in the temporal lobe*. Locations of electrodes exhibiting significantly different responses between sub-MIRC post and sub-MIRC images (n=39). Selective responses were mostly located in the temporal cortex (n=17). (****B****) Distribution of start times for selective responses for the sub-MIRC post vs. sub-MIRC comparison in the temporal cortex (median=252ms). The distributions of onset times for electrodes located in the frontal, parietal and occipital cortex are not shown since only n=5, n=6 and n=6 electrodes, respectively, were found.*

STAR Methods

Key resources table

Software and algorithms		
Python 3.12.7	Python Software Foundation	https://www.python.org/
Matlab R2024	The MathWorks, Inc., Natick, MA	https://www.mathworks.com
FreeSurfer 6	[86]	https://surfer.nmr.mgh.harvard.edu/
Intracranial Electrode Visualization (iELVis) Toolbox	[87]	https://github.com/iELVis/iELVis
generalized Directed Partial Coherence (gDPC)	[31,32]	
Custom code developed in this study	DOI: 10.5281/zenodo.14788055	https://kreimanlab.com/code/mirc/

Resource availability

Raw data and the code developed for data analysis are available at https://kreimanlab.com/code/mirc/ and also DOI: 10.5281/zenodo.14788055

Materials availability

This study did not use or generate any reagents.

Experimental model and study participant details

Participants were 12 patients (5 male, 11–43 years old, see **Table S2**) with pharmacologically-resistant epilepsy treated at Children's Hospital Boston (CHB) or John Hopkins Hospital (JHH). The patients were implanted with intracranial electrodes to localize seizure foci for potential surgical resection [29,88]. All procedures were approved by each hospital's institutional review board and were carried out with the participants' informed consent. Electrode types, numbers, and locations were driven solely by clinical considerations.

Methods

Psychophysics task

Participants had to identify grayscale images presented at the center of a Mac Pro 15-inch laptop's screen placed in front of them. Stimuli were presented with a uniform gray ([128, 128, 128]) background, at an estimated screen luminance of around 150 nits. The sequence of events within each trial is shown in **Figure 1A**. Participants were first presented with a black fixation cross on a gray screen. After 400ms, the fixation cross disappeared, and an image was presented at the center of the screen for 1s. Images were 200 × 200 pixels in size and subtended approximately 5x5 degrees of visual angle. Finally, patients were shown a blank screen with a question mark and asked to report verbally with a single word what they recognized in the image. The experimenter compared these single-word responses with a list of acceptable words for each image to assess correctness. The list of acceptable words was created by asking a different set of participants in the lab to describe the full object images with single words using unlimited presentation time. The participants' responses were recorded, and no feedback about their correctness was provided. In total, 5,444 images were presented across all participants.

Visual stimuli

The images presented in our experiment were a subset of those used in the original Ullman *et al.* study [26].The images were generated starting from a set of 10 images representing objects or object parts from ten different categories (**Figure 1B**: plane, ship, fly, eagle, horse, bike, car, eye, eyeglasses, and suit). For each image, Ullman *et al*. generated five descendants belonging to two types obtained by iteratively cropping it or resampling it at a lower resolution respectively. They operationally labeled an image a "MIRC"

451 if "it could be reliably identified by a human observer and none of its five descendants could reach a
452 recognition criterion of 50%" [26]. A non-recognizable descendant of a MIRC is referred to as "sub-MIRC".
453 Images could thus only post-hoc be labeled as MIRC or sub-MIRC. The combination of the similarity at the
454 pixel with the dramatic difference in recognition rates of MIRC and sub-MIRC stimuli make them ideal
455 candidates to probe the differences in neural processes between recognized and unrecognized stimuli.

456 Ullman *et al.*'s original behavioral experiment was run online on Amazon's Mechanical Turk and
457 sampled a large population of approximately 14,000 participants [26]. Comparisons were made across
458 participants who were exposed to each image only once. Our focus was to evaluate the neural responses
459 to those images and we therefore introduced several modifications to the task. In Ullman *et al.*'s
460 experiments, each participant viewed only one image. In our experiments, each participant was presented
461 with images from all the 10 categories ("object" condition in **Figure 1D**) together with three of its
462 descendants at progressively higher levels of degradation. To minimize adaptation effects, stimuli were
463 presented in a mini-block design paradigm. Within each mini-block, we presented stimuli belonging to two
464 out of the ten stimulus categories starting from the most degraded to the undegraded images ("object"
465 condition) (**Figures 1C**). The most degraded stimuli were presented again at the end of the mini-block ("sub-
466 MIRC post" condition). Each participant underwent 5 consecutive mini-blocks so as to present all 10
467 stimulus categories. The order of presentation of the 10 categories was randomized across participants.
468 For subject 1, stimuli were presented in a standard block design with no mini-blocks. In a separate
469 psychophysics experiment with 7 participants without epilepsy, we verified that this modified experimental
470 design did not alter recognition performance and yielded results similar to the original study (**Figure S2**).

471 Following Ullman *et al.* [26],for each category and participant, we labeled "MIRCs" all images whose
472 recognition performance was higher than 50% and "sub-MIRCs" all images that yielded a recognition rate
473 smaller than 50%. This step defined, on a participant-by-participant level, the threshold for which a
474 recognizable visual stimulus (i.e., a MIRC) becomes unrecognizable (i.e., a sub-MIRC). For each participant,
475 image categories for which this was not possible (i.e., that produced a recognition rate consistently higher
476 or lower than 50% at all levels of degradation) were excluded from further analyses. In the "MIRC" and
477 "sub-MIRC" blocks, each participant was shown each image for 10 times for a total of 200 trials (10
478 categories x 2 conditions (MIRC and sub-MIRC) x 10 repetitions). In the "object" and "sub-MIRC post"
479 blocks, each participant was shown each image for 5 times for a total of 100 trials (10 categories x 2
480 conditions (object and sub-MIRC post) x 10 repetitions). The original Ullman *et al* study only defined MIRC
481 and sub-MIRC *on average*, *across participants*. However, for the evaluation of neural responses, it is

essential to define whether a given participant recognized an image or not. For example, a given sub-MIRC image could yield, say, 15% recognition and the corresponding MIRC image could yield, say, 90% recognition, on average across participants, which would be consistent with the strong behavioral effects reported in Figure 1D and in the original study. However, here we are particularly interested in whether a given individual participant did or did not recognize a given image and it would thus not suffice to use the average behavioral assessments.

Neurophysiological recordings

Participants were implanted with either intracortical stereo electroencephalography (sEEG) depth electrodes or subdural electrocorticography (ECoG) electrodes (Ad-Tech, Racine, WI, USA). Depth electrodes contained from 6 to 16 recording sites. Each subdural grid or strip had from 4 to 128 recording sites with an inter-site distance of 1 cm. Each recording site was 2 mm in diameter. The number of recording sites per participant ranged from 83 to 229, for a total of 1,752 sites across all participants (see **Table S1** for the electrodes for which brain location could be recovered). All data were collected during periods without seizures. Data were recorded using XLTEK (Oakville, ON, Canada) or BioLogic (Knoxville, TN, USA) with sampling rates of 1,000 Hz 3or 2,000 Hz, depending on the hospital. For analysis purposes, all signals were down-sampled to 1,000 Hz.

Quantification and statistical analysis

Data Pre-processing

Data analyses were performed in Python. We followed the same pre-processing steps for the intracranial field potentials (IFPs) as in previous studies [29]. We first applied a notch filter at 60 Hz and harmonics, and we then low-pass filtered the signal at 100 Hz. We excluded from further analysis electrodes that showed evidence of electrical noise. Finally, to remove potential movement artifacts, we computed, on a per-electrode basis, the overall distribution of the total IFP power in all trials for each electrode (regardless of experimental condition) and excluded from further analyses those trials whose power was more than 4 standard deviations from the mean.

510

511 ## Electrode localization

512 Electrodes were localized by co-registering the preoperative magnetic resonance imaging (MRI)
513 with the postoperative computer tomography (CT) by means of the iELVis toolbox for Matlab [87]. For each
514 participant, the brain surface was reconstructed from the MRI, corrected for post-implant brain shift, and
515 assigned to one of 75 different regions in Freesurfer software [86] based on the 2009 atlas [29,89,90]. Depth
516 electrodes were assigned either to a subcortical structure or to gyri/sulci. The location of electrodes for
517 which the brain location could be recovered together with their average MNI coordinates is shown in **Table**
518 **S1**.

519 ## Data Analysis

520 **Comparison between conditions** – We first sorted the instantaneous values of the IFPs at time *t*, $IFP_j(t)$,
521 based on trial *j* and condition *c* (i.e., MIRC, sub-MIRC, object or sub-MIRC post). For each condition and
522 participant, we normalized all trials by subtracting the average across trials of the IFPs during the baseline
523 interval ([-200 50] ms before stimulus onset). For each contrast between two conditions *c1* and *c2* (e.g.,
524 MIRC vs sub-MIRC), we first identified the set of responsive electrodes, defined as those electrodes whose
525 $IFP_j(t)$ were statistically different from baseline at a $p<0.01$ level (Wilcoxon ranksum test) for at least 50
526 consecutive time points for either condition *c1* or condition *c2*. The length of this interval was selected so
527 as to keep the experiment-wide false discovery rate below the $p<0.05$ threshold throughout all our analyses
528 (see section "Bootstrapping analysis of the number of selective electrodes" and **Figure S5**). We defined
529 visually selective electrodes within the responsive electrodes as those whose distributions $IFP_{j,c1}(t)$ and
530 $IFP_{j,c2}(t)$ during conditions c1 and c2 respectively, were statistically different at a $p<0.01$ level for at least 50
531 consecutive time points. The latency of stimulus selectivity was defined as the first time point when the
532 statistical test was significant. We focused on two comparisons: MIRC vs. sub-MIRC and sub-MIRC post vs.
533 sub-MIRC in the time interval [50 550] ms after stimulus onset.

534

535 **Bootstrapping analysis of the number of selective electrodes** – To estimate the null-hypothesis distribution
536 of the number of significant electrodes yielded by a contrast between two conditions *c1* and *c2* we first
537 randomly shuffled, within each participant, the labels of the trials belonging to the conditions and we then
538 performed the analysis as detailed above ("Comparison between conditions"). We repeated these steps

for 500 times to estimate the null-hypothesis distribution. Comparison of the number of selective electrodes obtained in the two contrasts described here (MIRC vs sub-MIRC: 156 electrodes, and sub-MIRC post vs sub-MIRC: 39 electrodes) with these null-distributions shows that in both cases the false discovery rate (FDR) was < 0.05 (**Figure S5**).

Directional correlation – To assess the directional correlation between channels, we employed the time-varying generalized Partial Directed Coherence (gPDC) [31], which is an approach based on the Geweke-Granger causality framework [91,92]. Among many directional correlation estimation methods such as the Directed Transfer Function, the Partial Directed Coherence, and the multivariate Granger Causality [32,93,94], the gPDC has been proven to be the most effective estimator and to be robust with respect to the data normalization method [32,95,96]. Within the Granger causality framework, a time series ***x*** is directionally correlated to a time series ***y*** if the knowledge of past samples of ***x*** reduces the prediction error for the current sample of ***y***. The relation can be estimated by fitting, for each participant, a time-varying multivariate autoregressive (MVAR) model on the set of available electrodes. In our analyses, the order of the MVAR model was set to 40 (i.e., spanning a 40ms interval) to account for neurophysiologically plausible timing of interactions between areas. Among time-varying MVAR estimation methods, the GLKF outperformed other algorithms, such as the recursive least square, the multivariate adaptive autoregressive estimator, the classic Kalman filter, and the dual extended Kalman filter [97–100]. It should be noted that we fitted the GLKF on the raw IFPs (i.e. not low-pass filtered), as spurious correlations can arise when time series are filtered [101]. For each participant, we then used the MVAR model parameters to compute the gPDC between each possible pair of electrodes in the temporal and frontal lobe. We discounted pre-stimulus connectivity by removing from each trial and frequency the average connectivity estimated in the baseline interval. For each electrode pair, the gPDC is a function of time and frequency. We averaged the gPDCs values in the frequency domain to deal only with broadband temporal signals. We then used a cluster-based permutation test [102] to quantitatively compare the strength of the directional correlation from the temporal to the frontal lobe and vice versa across participants and channels. This analysis identified clusters of contiguous time points exhibiting consistent patterns, and permutation testing was applied to determine whether these clusters represented statistically significant deviations from chance.

Analysis of the latency of directional correlation – For each frontal electrode f_i, we conducted a cluster-based permutation test [102] to compare the mean directional correlation from all temporal electrodes to f_i against the mean directional correlation from f_i to all temporal electrodes. The first time point at which this difference was statistically significant, if present, represented the onset latency of a difference between the directed correlation to or from f_i. Latencies were then sorted into two sets, based on whether they corresponded to a higher gPDC from the temporal lobe to f_i or from f_i to the temporal lobe (the two distributions in **Figure 4B**). A subsequent Mann-Whitney U test was employed to assess the significance of the difference in latency distributions of the medians between these two sets.

References

1. Riesenhuber, M., and Poggio, T. (2000). Models of object recognition. Nat. Neurosci. *3*, 1199–1203.

2. Peissig, J.J., and Tarr, M.J. (2007). Visual object recognition: Do we know more now than we did 20 years ago? Annu. Rev. Psychol. *58*, 75–96. https://doi.org/10.1146/annurev.psych.58.102904.190114.

3. Biederman, I., and Gerhardstein, P.C. (1993). Recognizing depth-rotated objects: Evidence and conditions for three-dimensional viewpoint invariance. J. Exp. Psychol. Hum. Percept. Perform. *19*, 1162–1182. https://doi.org/10.1037/0096-1523.19.6.1162.

4. Biederman, I., and Cooper, E.E. (1991). Evidence for Complete Translational and Reflectional Invariance in Visual Object Priming. Perception *20*, 585–593. https://doi.org/10.1068/p200585.

5. Alais, D., Blake, R., and Lee, S.-G. (1998). Visual features that vary together over time group together over space. Nat. Neurosci. *1*, 160–164. https://doi.org/10.1038/414.

6. Gerbino, W., and Salmaso, D. (1987). The effect of amodal completion on sequential matching. Acta Psychol. (Amst). *65*, 25–46.

7. Rensink, R.A., and Enns, J.T. (1998). Early completion of occluded objects. Vision Res. *38*, 2489–2505. https://doi.org/10.1016/S0042-6989(98)00051-0.

8. Blake, R., and Lee, S.-H. (2005). The role of temporal structure in human vision. Behav. Cogn. Neurosci. Rev. *4*, 21–42. https://doi.org/10.1177/1534582305276839.

9. Snodgrass, J.G., and Feenan, K. (1990). Priming effects in picture fragment completion: Support for the perceptual closure hypothesis. J. Exp. Psychol. Gen. *119*, 276–296. https://doi.org/10.1037/0096-3445.119.3.276.

10. Foley, M.A., Foley, H.J., Durso, F.T., and Smith, N.K. (1997). Investigations of closure processes: What source-monitoring judgments suggest about what is “closing.” Mem. Cognit. *25*, 140–155. https://doi.org/10.3758/BF03201108.

11. Gollin, E.S. (1962). Factors Affecting the Visual Recognition of Incomplete Objects: A Comparative Investigation of Children and Adults. Percept. Mot. Skills *15*, 583–590. https://doi.org/10.2466/pms.1962.15.3.583.

12. Gauthier, I., and Tarr, M.J. (2016). Visual object recognition: Do we (finally) know more now than we did? Annu. Rev. Vis. Sci. *2*, 377–396. https://doi.org/10.1146/annurev-vision-111815-114621.

13. Ungerleider, L.G., and Bell, A.H. (2011). Uncovering the visual “ alphabet”: Advances in our understanding of object perception. Vision Res. *51*, 782–799. https://doi.org/10.1016/j.visres.2010.10.002.

14. Casile, A., and Giese, M.A. (2005). Critical features for the recognition of biological motion. J. Vis., 348–360. https://doi.org/10.1167/5.4.6.

15. Ullman, S., Vidal-Naquet, M., and Sali, E. (2002). Visual features of intermediate complexity and their use in classification. Nat. Neurosci. *5*, 682–687. https://doi.org/10.1038/nn870.

16. Gosselin, F., and Schyns, P.G. (2001). Bubbles: a technique to reveal the use of information in recognition tasks. Vision Res. *41*, 2261–2271. https://doi.org/10.1016/S0042-6989(01)00097-9.

17. Nielsen, K.J., Logothetis, N.K., and Rainer, G. (2006). Discrimination Strategies of Humans and Rhesus Monkeys for Complex Visual Displays. Curr. Biol. *16*, 814–820. https://doi.org/10.1016/j.cub.2006.03.027.

18. Gibson, B.M., Lazareva, O.F., Gosselin, F., Schyns, P.G., and Wasserman, E.A. (2007). Nonaccidental Properties Underlie Shape Recognition in Mammalian and Nonmammalian Vision. Curr. Biol. *17*, 336–340. https://doi.org/10.1016/j.cub.2006.12.025.

19. Kollmorgen, S., Nortmann, N., Schröder, S., and König, P. (2010). Influence of Low-Level Stimulus Features, Task Dependent Factors, and Spatial Biases on Overt Visual Attention. PLoS Comput. Biol. *6*, e1000791. https://doi.org/10.1371/journal.pcbi.1000791.

20. Tang, H., Buia, C., Madhavan, R., Crone, N.E., Madsen, J.R., Anderson, W.S., and Kreiman, G. (2014). Spatiotemporal dynamics underlying object completion in human ventral visual cortex. Neuron *83*, 736–748. https://doi.org/10.1016/j.neuron.2014.06.017.

21. Nielsen, K.J., Logothetis, N.K., and Rainer, G. (2006). Dissociation Between Local Field Potentials and Spiking Activity in Macaque Inferior Temporal Cortex Reveals Diagnosticity-Based Encoding of Complex Objects. J. Neurosci. *26*, 9639–9645. https://doi.org/10.1523/JNEUROSCI.2273-06.2006.

22. Snodgrass, J.G., and Corwin, J. (1988). Perceptual Identification Thresholds for 150 Fragmented Pictures from the Snodgrass and Vanderwart Picture Set. Percept. Mot. Skills *67*, 3–36. https://doi.org/10.2466/pms.1988.67.1.3.

23. Gruber, T., Trujillo-Barreto, N.J., Giabbiconi, C.-M., Valdés-Sosa, P.A., and Müller, M.M. (2006). Brain electrical tomography (BET) analysis of induced gamma band responses during a simple object recognition task. Neuroimage *29*, 888–900. https://doi.org/10.1016/j.neuroimage.2005.09.004.

24. Grutzner, C., Uhlhaas, P.J., Genc, E., Kohler, A., Singer, W., and Wibral, M. (2010). Neuroelectromagnetic Correlates of Perceptual Closure Processes. J. Neurosci. *30*, 8342–8352. https://doi.org/10.1523/JNEUROSCI.5434-09.2010.

25. Tallon-Baudry, C., and Bertrand, O. (1999). Oscillatory gamma activity in humans and its role in object representation. Trends Cogn. Sci. *3*, 151–162. https://doi.org/10.1016/S1364-6613(99)01299-1.

26. Ullman, S., Assif, L., Fetaya, E., and Harari, D. (2016). Atoms of recognition in human and computer vision. Proc. Natl. Acad. Sci. USA *113*, 2744–2749. https://doi.org/10.1073/pnas.1513198113.

27. Srivastava, S., Ben-Yosef, G., and Boix, X. (2019). Minimal images in deep neural networks: Fragile object recognition in natural images. In 7th International Conference on Learning Representations (ICLR 2019).

28. VanRullen, R. (2011). Four common conceptual fallacies in mapping the time course of recognition. Front. Psychol. *2*, 1–6. https://doi.org/10.3389/fpsyg.2011.00365.

29. Liu, H., Agam, Y., Madsen, J.R., and Kreiman, G. (2009). Timing, timing, timing: Fast decoding of object information from intracranial field potentials in human visual cortex. Neuron *62*, 281–290. https://doi.org/10.1016/j.neuron.2009.02.025.

30. Hartigan, J.A., and Hartigan, P.M. (1985). The Dip Test of Unimodality. Ann. Stat. *13*, 1403–1433. https://doi.org/10.1214/aos/1176346577.

31. Baccalá, L.A., Sameshima, K., and Takahashi, D.Y. (2007). Generalized Partial Directed Coherence. In 2007 15th International Conference on Digital Signal Processing (IEEE), pp. 163–166. https://doi.org/10.1109/ICDSP.2007.4288544.

32. Baccalá, L.A., and Sameshima, K. (2001). Partial directed coherence: a new concept in neural structure determination. Biol. Cybern. *84*, 463–474. https://doi.org/10.1007/PL00007990.

33. Schall, J.D. (2015). Visuomotor Functions in the Frontal Lobe. Annu. Rev. Vis. Sci. *1*, 469–498. https://doi.org/10.1146/annurev-vision-082114-035317.

34. Wilson, F.A.W., Scalaidhe, S.P.Ó., and Goldman-Rakic, P.S. (1993). Dissociation of Object and Spatial Processing Domains in Primate Prefrontal Cortex. Science (80-.). *260*, 1955–1958. https://doi.org/10.1126/science.8316836.

35. Meyer, T., Qi, X.-L., Stanford, T.R., and Constantinidis, C. (2011). Stimulus Selectivity in Dorsal and Ventral Prefrontal Cortex after Training in Working Memory Tasks. J. Neurosci. *31*, 6266–6276. https://doi.org/10.1523/JNEUROSCI.6798-10.2011.

36. Ó Scalaidhe, S.P., Wilson, F.A.W., and Goldman-Rakic, P.S. (1997). Areal segregation of face-processing neurons in prefrontal cortex. Science (80-.). *278*, 1135–1138. https://doi.org/10.1126/science.278.5340.1135.

37. Rainer, G., and Ranganath, C. (2002). Coding of objects in the prefrontal cortex in monkeys and humans. Neuroscientist *8*, 6–11. https://doi.org/10.1177/107385840200800104.

38. Rainer, G., and Miller, E.K. (2000). Effects of visual experience on the representation of objects in the prefrontal cortex. Neuron *27*, 179–189.

39. Meyers, E.M., Freedman, D.J., Kreiman, G., Miller, E.K., and Poggio, T. (2008). Dynamic Population Coding of Category Information in Inferior Temporal and Prefrontal Cortex. J. Neurophysiol. *100*, 1407–1419. https://doi.org/10.1152/jn.90248.2008.

40. Wutz, A., Loonis, R., Roy, J.E., Donoghue, J.A., and Miller, E.K. (2018). Different Levels of Category Abstraction by Different Dynamics in Different Prefrontal Areas. Neuron *97*, 716-726.e8. https://doi.org/10.1016/j.neuron.2018.01.009.

41. Martinovic, J., Gruber, T., Hantsch, A., and Müller, M.M. (2008). Induced gamma-band activity is related to the time point of object identification. Brain Res. *1198*, 93–106. https://doi.org/10.1016/j.brainres.2007.12.050.

42. Stuss, D.T., Picton, T.W., Cerri, A.M., Leech, E.E., and Stethem, L.. (1992). Perceptual closure and object identification: Electrophysiological responses to incomplete pictures. Brain Cogn. *19*, 253–266. https://doi.org/10.1016/0278-2626(92)90047-P.

43. Bar, M., Kassam, K.S., Ghuman, A.S., Boshyan, J., Schmid, A.M., Dale, A.M., Hamalainen, M.S., Marinkovic, K., Schacter, D.L., Rosen, B.R., et al. (2006). Top-down facilitation of visual recognition. Proc. Natl. Acad. Sci. *103*, 449–454. https://doi.org/10.1073/pnas.0507062103.

44. Fyall, A.M., El-Shamayleh, Y., Choi, H., Shea-Brown, E., and Pasupathy, A. (2017). Dynamic representation of partially occluded objects in primate prefrontal and visual cortex. Elife *6*, 1–25. https://doi.org/10.7554/eLife.25784.

45. Kar, K., and DiCarlo, J.J. (2021). Fast Recurrent Processing via Ventrolateral Prefrontal Cortex Is Needed by the Primate Ventral Stream for Robust Core Visual Object Recognition. Neuron *109*, 164-176.e5. https://doi.org/10.1016/j.neuron.2020.09.035.

46. Romanski, L.M., and Chafee, M. V (2021). A View from the Top: Prefrontal Control of Object Recognition. Neuron *109*, 6–8. https://doi.org/10.1016/j.neuron.2020.12.014.

47. Seger, C.A., and Miller, E.K. (2010). Category Learning in the Brain. Annu. Rev. Neurosci. *33*, 203–219. https://doi.org/10.1146/annurev.neuro.051508.135546.

48. Miller, E.K., Freedman, D.J., and Wallis, J.D. (2002). The prefrontal cortex: categories, concepts and cognition. Philos. Trans. R. Soc. London. Ser. B Biol. Sci. *357*, 1123–1136. https://doi.org/10.1098/rstb.2002.1099.

49. Miller, E.K., Nieder, A., Freedman, D.J., and Wallis, J.D. (2003). Neural correlates of categories and concepts. Curr. Opin. Neurobiol. *13*, 198–203. https://doi.org/10.1016/S0959-4388(03)00037-0.

50. Freedman, D.J., Riesenhuber, M., Poggio, T., and Miller, E.K. (2001). Categorical Representation of Visual Stimuli in the Primate Prefrontal Cortex. Science (80-.). *291*, 312–316. https://doi.org/10.1126/science.291.5502.312.

51. Freedman, D.J., Riesenhuber, M., Poggio, T., and Miller, E.K. (2002). Visual Categorization and the Primate Prefrontal Cortex: Neurophysiology and Behavior. J. Neurophysiol. *88*, 929–941. https://doi.org/10.1152/jn.2002.88.2.929.

52. Bertrand, J.-A., Tremblay, J., Lassonde, M., Vannasing, P., Khoa Nguyen, D., Robert, M., Bouthillier, A., and Lepore, F. (2013). Induced gamma-band response to fragmented images: An intracranial EEG study. Neuropsychologia *51*, 584–591. https://doi.org/10.1016/j.neuropsychologia.2013.01.002.

53. Gruber, L.Z., Ullman, S., and Ahissar, E. (2021). Oculo-retinal dynamics can explain the perception of minimal recognizable configurations. Proc. Natl. Acad. Sci. U. S. A. *118*, e2022792118. https://doi.org/10.1073/pnas.2022792118.

54. Chao, Z.C., Takaura, K., Wang, L., Fujii, N., and Dehaene, S. (2018). large-scale cortical networks for hierarchical prediction and prediction error in the primate brain. Neuron *100*, 1252-1266.e3. https://doi.org/10.2139/ssrn.3188377.

55. Jensen, O., Bonnefond, M., Marshall, T.R., and Tiesinga, P. (2015). Oscillatory mechanisms of feedforward and feedback visual processing. Trends Neurosci. *38*, 192–194. https://doi.org/10.1016/j.tins.2015.02.006.

56. Parto-Dezfouli, M., Vezoli, J., Bosman, C.A., and Fries, P. (2023). Enhanced behavioral performance through interareal gamma and beta synchronization. Cell Rep. *42*, 113249. https://doi.org/10.1016/j.celrep.2023.113249.

57. Bastos, A.M., Vezoli, J., Bosman, C.A., Schoffelen, J.-M., Oostenveld, R., Dowdall, J.R., De Weerd, P., Kennedy, H., and Fries, P. (2015). Visual areas exert feedforward and feedback influences through distinct frequency channels. Neuron *85*, 390–401. https://doi.org/10.1016/j.neuron.2014.12.018.

58. Loh, K.K., Petrides, M., Hopkins, W.D., Procyk, E., and Amiez, C. (2017). Cognitive control of vocalizations in the primate ventrolateral-dorsomedial frontal (VLF-DMF) brain network. Neurosci. Biobehav. Rev. *82*, 32–44. https://doi.org/10.1016/j.neubiorev.2016.12.001.

59. Doniger, G.M., Foxe, J.J., Murray, M.M., Higgins, B.A., Snodgrass, J.G., Schroeder, C.E., and Javitt, D.C. (2000). Activation Timecourse of Ventral Visual Stream Object-recognition Areas: High Density Electrical Mapping of Perceptual Closure Processes. J. Cogn. Neurosci. *12*, 615–621. https://doi.org/10.1162/089892900562372.

60. Sehatpour, P., Molholm, S., Schwartz, T.H., Mahoney, J.R., Mehta, A.D., Javitt, D.C., Stanton, P.K., and Foxe, J.J. (2008). A human intracranial study of long-range oscillatory coherence across a frontal-occipital-hippocampal brain network during visual object processing. Proc. Natl. Acad. Sci. U. S. A. *105*, 4399–4404. https://doi.org/10.1073/pnas.0708418105.

61. Gruber, T., Maess, B., Trujillo-Barreto, N.J., and Müller, M.M. (2008). Sources of synchronized induced Gamma-Band responses during a simple object recognition task: A replication study in human MEG. Brain Res. *1196*, 74–84. https://doi.org/10.1016/j.brainres.2007.12.037.

62. Namima, T., and Pasupathy, A. (2021). Encoding of partially occluded and occluding objects in primate inferior temporal cortex. J. Neurosci. *41*, 5662–5666. https://doi.org/10.1523/JNEUROSCI.2992-20.2021.

63. Kosai, Y., El-Shamayleh, Y., Fyall, A.M., and Pasupathy, A. (2014). The role of visual area V4 in the discrimination of partially occluded shapes. J. Neurosci. *34*, 8570–8584. https://doi.org/10.1523/JNEUROSCI.1375-14.2014.

64. Kovács, G., Vogels, R., and Orban, G.A. (1995). Selectivity of macaque inferior temporal neurons for partially occluded shapes. J. Neurosci. *15*, 1984–1997. https://doi.org/10.1523/jneurosci.15-03-01984.1995.

65. Holzinger, Y., Ullman, S., Harari, D., Behrmann, M., and Avidan, G. (2019). Minimal recognizable configurations elicit category-selective responses in higher order visual cortex. J. Cogn. Neurosci. *31*, 1354–1367. https://doi.org/10.1162/jocn_a_01420.

66. Tovee, M.J., Rolls, E.T., and Ramachandran, V.S. (1996). Rapid visual learning in neurones of the primate temporal visual cortex. Neuroreport *7*, 2757–2760. https://doi.org/10.1097/00001756-199611040-00070.

67. Chalupa, L.M., and Werner, J.S. (2003). The visual neurosciences (Bradford).

68. Hung, C.P., Kreiman, G., Poggio, T., and DiCarlo, J.J. (2005). Fast readout of object identity from macaque inferior temporal cortex. Science (80-.). *310*, 863–866. https://doi.org/10.1126/science.1117593.

69. Thorpe, S., Fize, D., and Marlot, C. (1996). Speed of processing in the human visual system. Nature *381*, 520–522. https://doi.org/10.1038/381520a0.

70. Harari, D., Benoni, H., and Ullman, S. (2020). Object recognition at the level of minimal images develops for up to seconds of presentation time. J. Vis. *20*, 266. https://doi.org/10.1167/jov.20.11.266.

71. Tang, H., Schrimpf, M., Lotter, W., Moerman, C., Paredes, A., Caro, J.O., Hardesty, W., Cox, D., and Kreiman, G. (2018). Recurrent computations for visual pattern completion. Proc. Natl. Acad. Sci. USA *115*, 8835–8840. https://doi.org/10.1073/pnas.1719397115.

72. Quiroga, R.Q., Reddy, L., Kreiman, G., Koch, C., and Fried, I. (2005). Invariant visual representation by single neurons in the human brain. Nature *435*, 1102–1107. https://doi.org/10.1038/nature03687.

73. Mormann, F., Kornblith, S., Quiroga, R.Q., Kraskov, A., Cerf, M., Fried, I., and Koch, C. (2008). Latency and Selectivity of Single Neurons Indicate Hierarchical Processing in the Human Medial Temporal Lobe. J. Neurosci. *28*, 8865–8872. https://doi.org/10.1523/JNEUROSCI.1640-08.2008.

74. Rey, H.G., Fried, I., and Quian Quiroga, R. (2014). Timing of Single-Neuron and Local Field Potential Responses in the Human Medial Temporal Lobe. Curr. Biol. *24*, 299–304.

https://doi.org/10.1016/j.cub.2013.12.004.

75. Quiroga, R.Q., Mukame, R., Isham, E.A., Malach, R., and Fried, I. (2008). Human single-neuron responses at the threshold of conscious recognition. Proc. Natl. Acad. Sci. U. S. A. *105*, 3599–3604. https://doi.org/10.1073/pnas.0707043105.

76. Bova, S.M., Fazzi, E., Giovenzana, A., Montomoli, C., Signorini, S.G., Zoppello, M., and Lanzi, G. (2007). The Development of Visual Object Recognition in School-Age Children. Dev. Neuropsychol. *31*, 79–102. https://doi.org/10.1207/s15326942dn3101_5.

77. Huber, L.S., Geirhos, R., and Wichmann, F.A. (2023). The developmental trajectory of object recognition robustness: Children are like small adults but unlike big deep neural networks. J. Vis. *23*, 1–30. https://doi.org/10.1167/jov.23.7.4.

78. Fukushima, K. (1980). Neocognitron: A self-organizing neural network model for a mechanism of pattern recognition unaffected by shift in position. Biol. Cybern. *36*, 193–202. https://doi.org/10.1007/BF00344251.

79. Riesenhuber, M., and Poggio, T. (1999). Hierarchical models of object recognition in cortex. Nat. Neurosci. *2*, 1019–1025. https://doi.org/10.1038/14819.

80. Krizhevsky, A., Sutskever, I., and Hinton, G.E. (2012). ImageNet classification with deep convolutional neural networks. In Advances in Neural Information Processing Systems 25 (NIPS 2012).

81. Krizhevsky, A., Sutskever, I., and Hinton, G.E. (2017). ImageNet classification with deep convolutional neural networks. Commun. ACM *60*, 84–90. https://doi.org/10.1145/3065386.

82. Rajalingham, R., Issa, E.B., Bashivan, P., Kar, K., Schmidt, K., and DiCarlo, J.J. (2018). Large-scale, high-resolution comparison of the core visual object recognition behavior of humans, monkeys, and state-of-the-art deep artificial neural networks. J. Neurosci. *38*, 7255–7269. https://doi.org/10.1523/JNEUROSCI.0388-18.2018.

83. Yamins, D.L.K., Hong, H., Cadieu, C.F., Solomon, E.A., Seibert, D., and Dicarlo, J.J. (2014). Performance-optimized hierarchical models predict neural responses in higher visual cortex. Proc. Natl. Acad. Sci. U. S. A. https://doi.org/10.1073/pnas.1403112111.

84. Serre, T. (2019). Deep Learning: The Good, the Bad, and the Ugly. Annu. Rev. Vis. Sci. *5*, 399–426. https://doi.org/10.1146/annurev-vision-091718-014951.

85. Kreiman, G., and Serre, T. (2020). Beyond the feedforward sweep: feedback computations in the visual cortex. Ann. N. Y. Acad. Sci. *1464*, 222–241. https://doi.org/10.1111/nyas.14320.

86. Dale, A.M., Fischl, B., and Sereno, M.I. (1999). Cortical Surface-Based Analysis. Neuroimage *9*, 179–194. https://doi.org/10.1006/nimg.1998.0395.

87. Groppe, D.M., Bickel, S., Dykstra, A.R., Wang, X., Mégevand, P., Mercier, M.R., Lado, F.A., Mehta, A.D., and Honey, C.J. (2017). iELVis: An open source MATLAB toolbox for localizing and visualizing human intracranial electrode data. J. Neurosci. Methods *281*, 40–48. https://doi.org/10.1016/j.jneumeth.2017.01.022.

88. Ojemann, G.A. (1997). Treatment of temporal lobe epilepsy. Annu. Rev. Med. *48*, 317–328. https://doi.org/10.1146/annurev.med.48.1.317.

89. Destrieux, C., Fischl, B., Dale, A., and Halgren, E. (2010). Automatic parcellation of human cortical gyri and sulci using standard anatomical nomenclature. Neuroimage *53*, 1–15.

https://doi.org/10.1016/j.neuroimage.2010.06.010.

90. Dykstra, A.R., Chan, A.M., Quinn, B.T., Zepeda, R., Keller, C.J., Cormier, J., Madsen, J.R., Eskandar, E.N., and Cash, S.S. (2012). Individualized localization and cortical surface-based registration of intracranial electrodes. Neuroimage *59*, 3563–3570. https://doi.org/10.1016/j.neuroimage.2011.11.046.

91. Geweke, J. (1982). Measurement of Linear Dependence and Feedback between Multiple Time Series. J. Am. Stat. Assoc. *77*, 304–313. https://doi.org/10.1080/01621459.1982.10477803.

92. Granger, C.W.J. (1969). Investigating causal relations by econometric models and cross-spectral methods. Econometrica *37*, 424–438.

93. Kamiński, M., Ding, M., Truccolo, W.A., and Bressler, S.L. (2001). Evaluating causal relations in neural systems: Granger causality, directed transfer function and statistical assessment of significance. Biol. Cybern. *85*, 145–157. https://doi.org/10.1007/s004220000235.

94. Wen, X., Rangarajan, G., and Ding, M. (2013). Is Granger causality a viable technique for analyzing FMRI data? PLoS One *8*, e67428. https://doi.org/10.1371/journal.pone.0067428.

95. Gürkan, G., Akan, A., and Seyhan, T.Ö. (2014). Analysis of brain connectivity changes after propofol injection by generalized partial directed coherence. Digit. Signal Process. *25*, 156–163. https://doi.org/10.1016/j.dsp.2013.11.011.

96. Taxidis, J., Coomber, B., Mason, R., and Owen, M. (2010). Assessing cortico-hippocampal functional connectivity under anesthesia and kainic acid using generalized partial directed coherence. Biol. Cybern. *102*, 327–340. https://doi.org/10.1007/s00422-010-0370-1.

97. Cometa, A., D'Orio, P., Revay, M., Micera, S., and Artoni, F. (2021). Stimulus evoked causality estimation in stereo-EEG. J. Neural Eng. *18*, 056041. https://doi.org/10.1088/1741-2552/ac27fb.

98. Ghumare, E.G., Schrooten, M., Vandenberghe, R., and Dupont, P. (2018). A time-varying connectivity analysis from distributed EEG sources: A simulation study. Brain Topogr. *31*, 721–737. https://doi.org/10.1007/s10548-018-0621-3.

99. Milde, T., Leistritz, L., Astolfi, L., Miltner, W.H.R., Weiss, T., Babiloni, F., and Witte, H. (2010). A new Kalman filter approach for the estimation of high-dimensional time-variant multivariate AR models and its application in analysis of laser-evoked brain potentials. Neuroimage *50*, 960–969. https://doi.org/10.1016/j.neuroimage.2009.12.110.

100. Pagnotta, M.F., and Plomp, G. (2018). Time-varying MVAR algorithms for directed connectivity analysis: Critical comparison in simulations and benchmark EEG data. PLoS One *13*, e0198846. https://doi.org/10.1371/journal.pone.0198846.

101. Florin, E., Gross, J., Pfeifer, J., Fink, G.R., and Timmermann, L. (2010). The effect of filtering on Granger causality based multivariate causality measures. Neuroimage *50*, 577–588. https://doi.org/10.1016/j.neuroimage.2009.12.050.

102. Nichols, T., and Holmes, A. (2004). Nonparametric Permutation Tests for Functional Neuroimaging. In Human Brain Function (Elsevier), pp. 887–910. https://doi.org/10.1016/B978-012264841-0/50048-2.

Figure 1

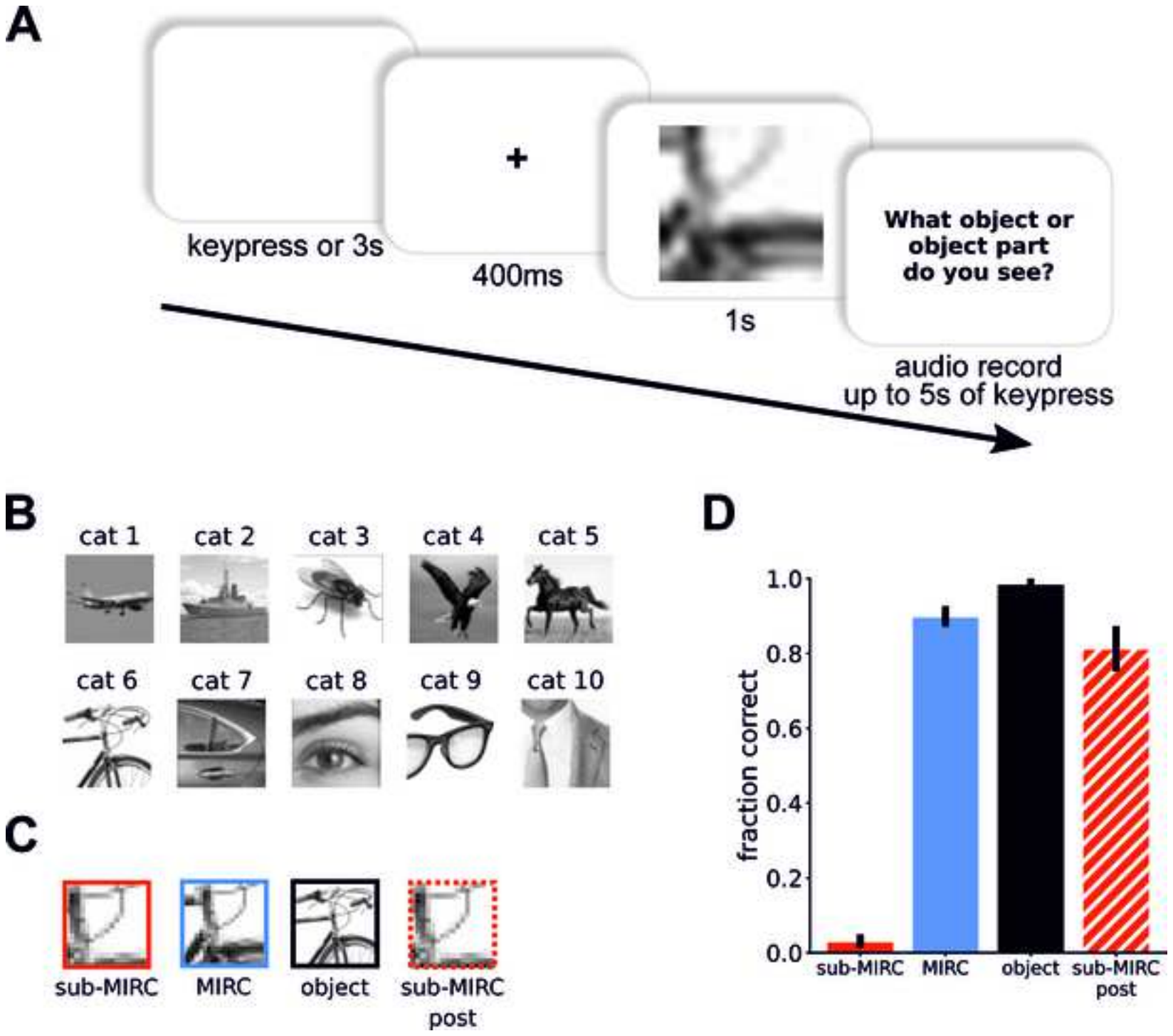

Figure 2

Click here to access/download;Figure;Figure_2.tif

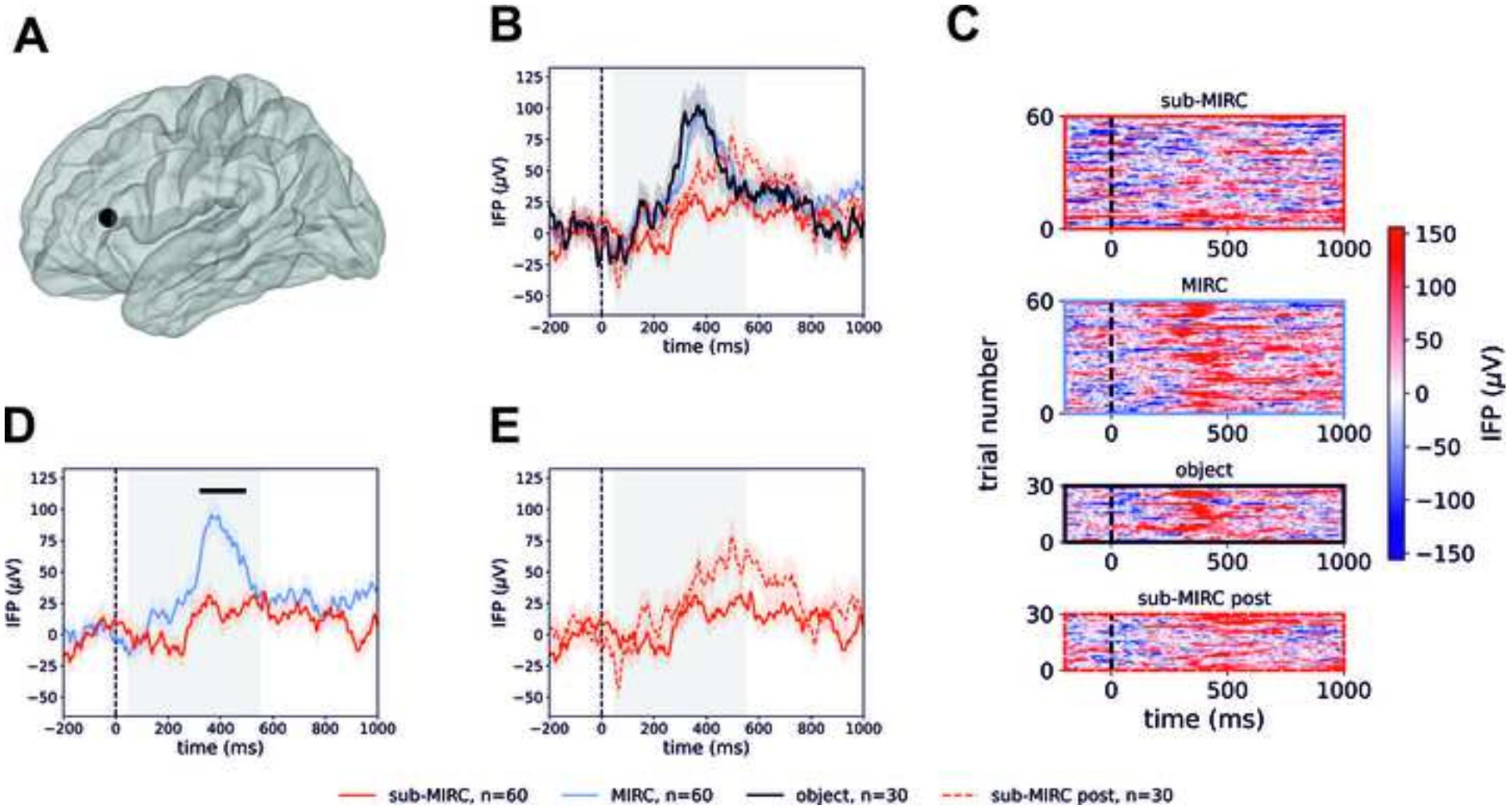

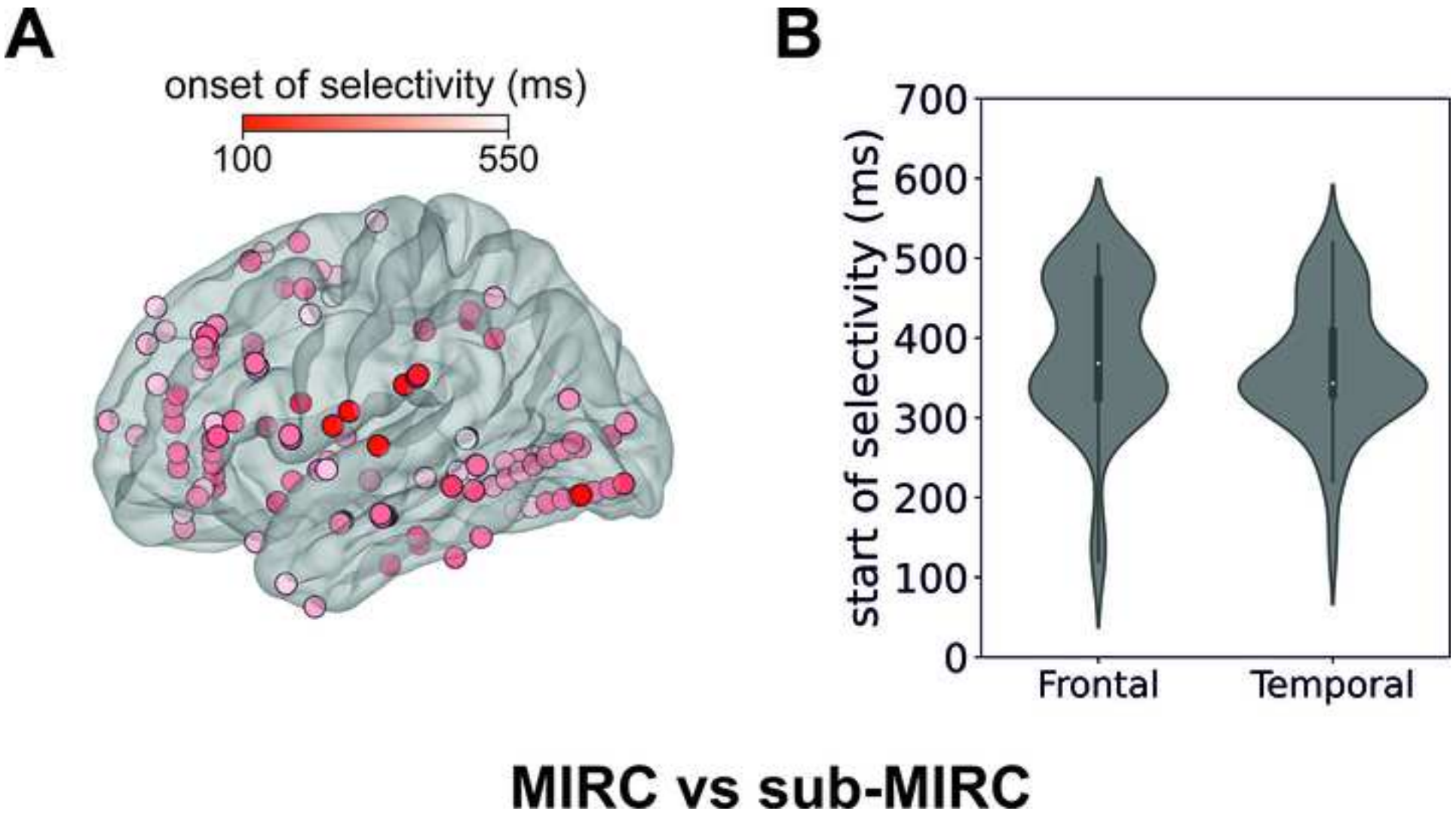

Figure 4

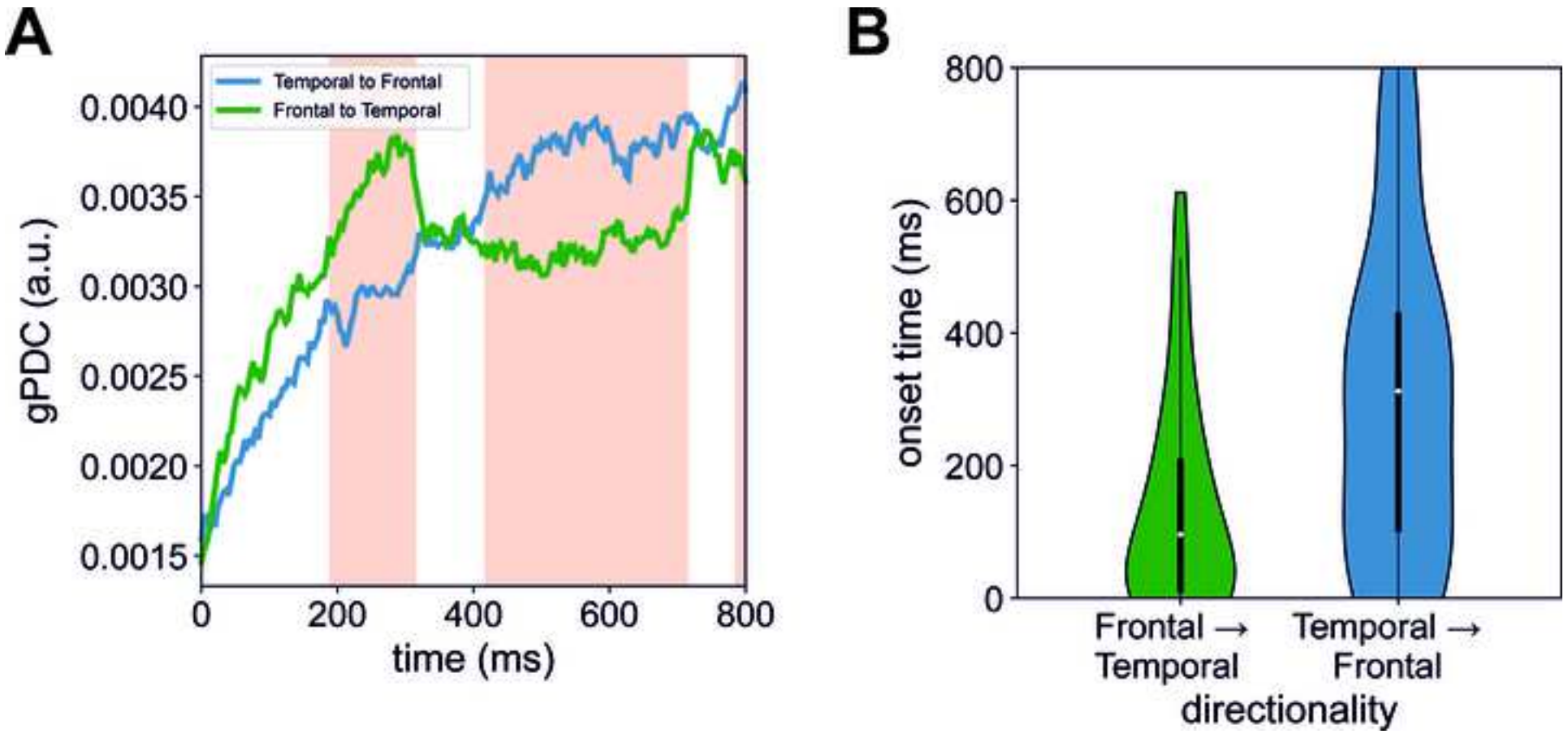

Figure 5

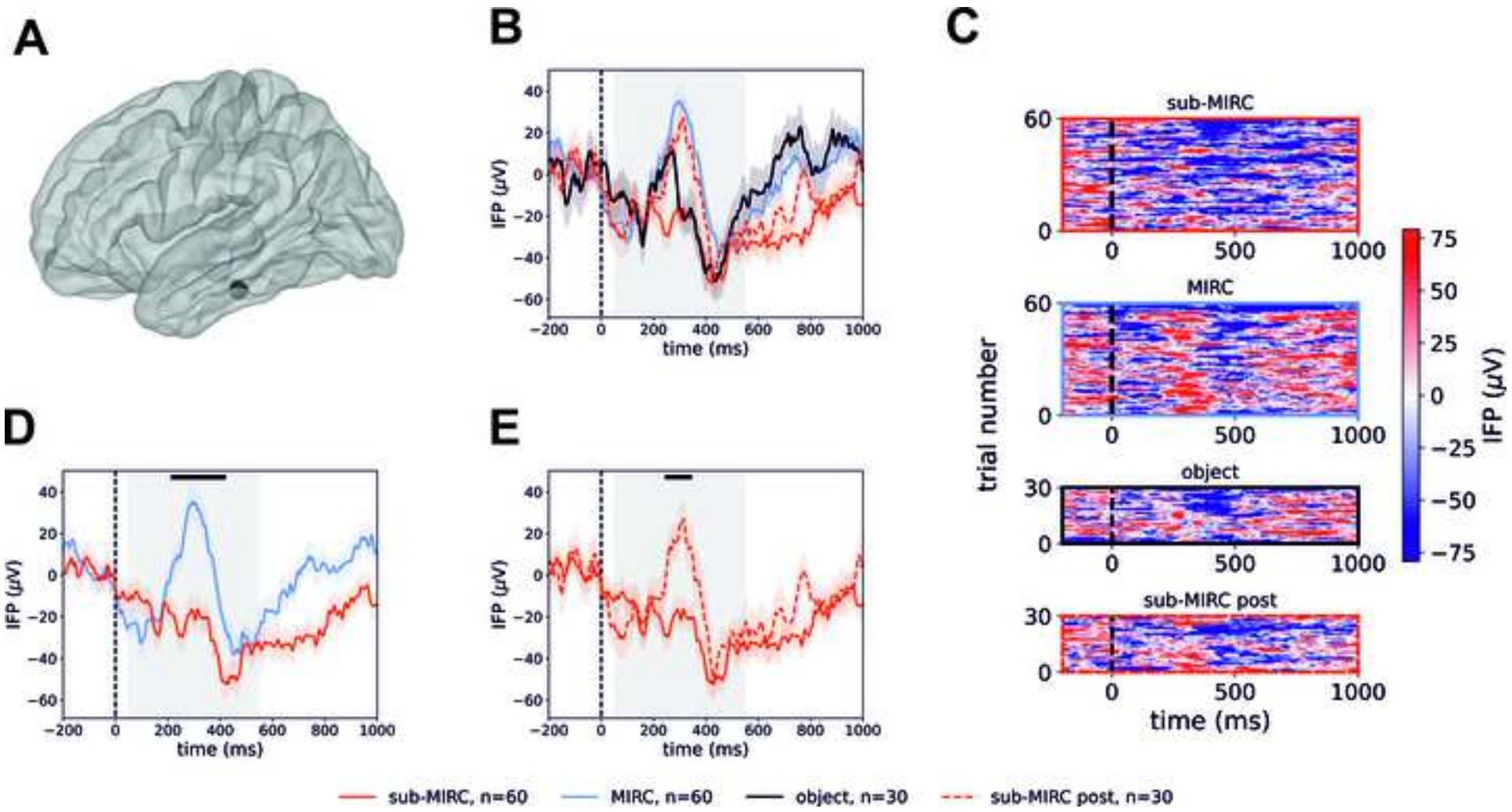

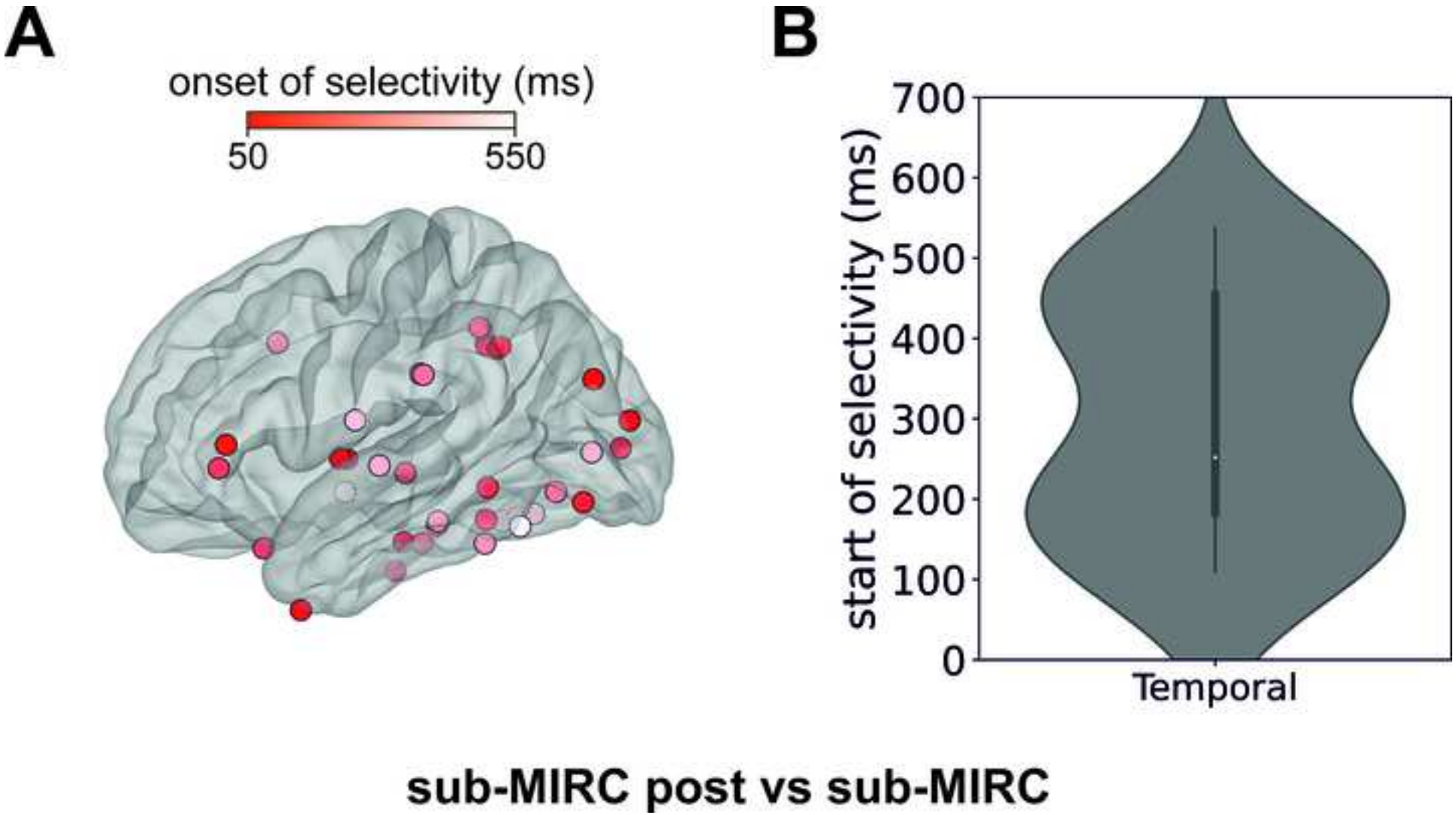

Casile *et al*, **Neural correlates of minimal recognizable configurations in the human brain**

Supplementary Tables

Region name	# Electrodes	Average MNI coordinates
G_temporal_middle	112	-60.82 -28.94 -12.43
G_front_middle	94	-37.68 30.46 32.94
G_front_sup	93	-9.95 23.86 39.87
G_temp_sup-Lateral	93	-60.7 -14.49 -4.11
G_occipital_middle	83	-35.48 -70.6 19.95
G_temporal_inf	67	-49.2 -26.57 -27.32
G_front_inf-Opercular	56	-48.92 12.29 10.84
S_temporal_inf	53	-49.73 -31.02 -17.01
Pole_occipital	51	-38.39 -35.8 21.38
G_pariet_inf-Supramar	50	-59.07 -35.03 30.91
S_temporal_sup	48	-46.44 -31.35 -2.51
G_oc-temp_med-Parahip	47	-27.73 -19.02 -19.4
G_precentral	42	-53.13 -0.39 36.9
S_front_inf	37	-37.91 24.89 23.38
G_front_inf-Triangul	33	-49.65 30.37 5.42
G&S_subcentral	31	-60.54 -4.83 15.96
G_pariet_inf-Angular	30	-44.01 -59.68 31.56
G&S_occipital_inf	29	-44.26 -60.85 13.45
G_orbital	29	-30.64 29.09 -16.97
G_postcentral	29	-52.57 -18.91 49.71
S_front_sup	27	-27.75 21.35 39.98
G_insular_short	26	-37.45 6.43 -4.04
S_circular_insula_inf	26	-40.51 -7.9 -11.32
S_collat_transv_ant	26	-37.78 -18.28 -22.26
Pole_temporal	25	-35.45 4.53 -39.32
S_orbital-H_Shaped	23	-36.44 35.96 -9.55
G&S_cingul-Ant	21	-14.14 41.5 4.38
S_circular_insula_sup	20	-34.17 2.58 6.54
G_oc-temp_lat-fusifor	17	-35.92 -45.83 -20.19
G&S_cingul-Mid-Ant	15	-11.67 19.98 22.99
S_oc-temp_lat	15	-44.79 -28. -22.56
G_temp_sup-Plan_tempo	13	-56.33 -37.03 8.31
S_front_middle	13	-29.85 39.74 14.51
S_postcentral	13	-31.77 -37.65 46.61
G_rectus	12	-6.01 48.56 -24.35
G_temp_sup-Plan_polar	11	-35.26 2.91 -21.76
S_pericallosal	11	-14.76 -30.52 12.26
S_precentral-inf-part	11	-41.99 9.23 22.37
G&S_frontomargin	10	-35.82 56.54 -8.87
G_occipital_sup	10	-20.03 -29.79 38.33
Lat_Fis-post	10	-44.36 -31.54 9.66
G&S_cingul-Mid-Post	9	-6.15 -20.08 35.88
G_oc-temp_med-Lingual	8	-10.37 -75.97 -8.28
G_precuneus	8	-2.76 -46.64 43.85
G_temp_sup-G_T_transv	8	-47.18 -13.58 9.09
S_intrapariet&P_trans	8	-36.38 -49.21 42.74
S_occipital_ant	7	-40.67 -66.72 -1.82
S_circular_insula_ant	6	-42.21 15.35 3.26
S_orbital_lateral	6	-53.85 32.58 13.59
G_Ins_lg&S_cent_ins	4	-34.72 1.59 -13.29
S_orbital_med-olfact	4	-10.49 38.35 -16.48
G&S_paracentral	3	-13.69 -42.52 62.77
G_parietal_sup	3	-36.53 -44.6 50.28
Lat_Fis-ant-Horizont	3	-32.23 33.54 -2.08
Lat_Fis-ant-Vertical	3	-46.15 20.54 12.04
S_oc-temp_med&Lingual	3	-34.48 -31.46 -15.18
S_suborbital	3	-12.17 44.2 -10.19
G&S_transv_frontopol	2	-9.95 68.48 -0.23
G_cuneus	2	-2.1 -82.47 11.71
G_front_inf-Orbital	2	-45.57 32.29 -15.75
S_collat_transv_post	2	-35.47 -82.49 -9.56
S_interm_prim-Jensen	2	-52.77 -52.5 28.19
S_calcarine	1	-10.39 -87.65 5.48
S_central	1	-24.11 -32.65 43.7
S_cingul-Marginalis	1	-5.2 -30.89 49.31
S_oc_middle&Lunatus	1	-28.2 -91.2 0.41
S_oc_sup&transversal	1	-19.77 -91.18 17.07
S_temporal_transverse	1	-50.2 -22.5 4.98

Table S1 - Anatomical locations of all electrodes for which brain localization could be computed*, Related to STAR Methods.*

Participant #	Age	Gender	# Electrodes
1	17	M	229
2	25	M	190
3	18	F	83
4	15	F	212
5	35	F	125
6	26	F	104
7	12	M	96
8	43	F	181
9	22	F	122
10	11	F	158
11	21	M	94
12	12	M	158

***Table S2 - Information about the 12 patients that participated in the study**, Related to STAR Methods.*

Participant #	Object	MIRC	subMIRC	subMIRC post
1	25	50	50	20
2	25	50	50	25
3	30	60	60	30
4	25	50	50	25
5	30	60	60	20
6	15	30	30	25
7	25	50	50	15
8	15	30	30	20
9	30	60	60	30
10	30	60	60	30
11	30	60	60	35
12	10	20	20	10

Table S3 - Number of trials that we considered in our analysis per condition for each participant, *Related to STAR Methods.*

Supplementary Figures

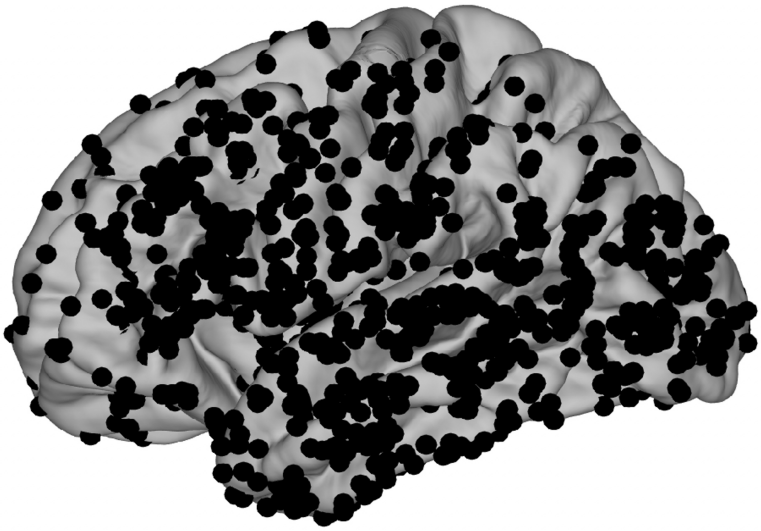

Figure S1 – Locations of recorded sites for which we could recover MNI coordinates across our cohort of patients *(n=12, see also* ***Table S1****), Related to* ***Figure 3, 6****, and STAR Methods.*

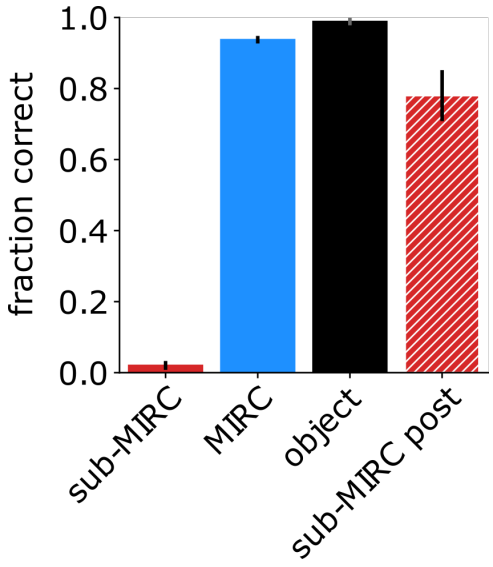

Figure S2 – Results of a behavioral study with 7 participants without epilepsy, *Related to* ***Figure 1*** *and STAR Methods. The format and conventions are as in* ***Figure 1D****.*

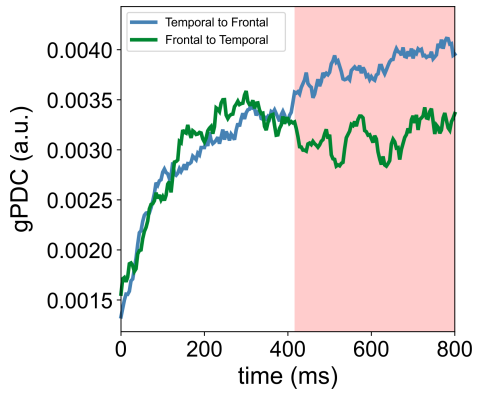

Figure S3 – Temporal dynamics of the functional interactions between temporal and frontal areas during the perception of sub-MIRC stimuli*, Related to* ***Figure 4.*** *The panel shows the strength, as assessed by generalized Partial Directed Coherence (gDPC, Baccalá et al., 2007), of the temporal to frontal (green curve) and frontal to temporal (blue curve) functional interactions measured in participants (n=6) that had at least 2 responsive electrodes in both the temporal and frontal lobe. The curves represent the average gPDC obtained from n=3639 pairs of frontal and temporal electrodes respectively. Standard errors are shown but they are too small to be visible. Red-shaded areas mark intervals where the interactions in one direction are significantly stronger than in the opposite direction.*

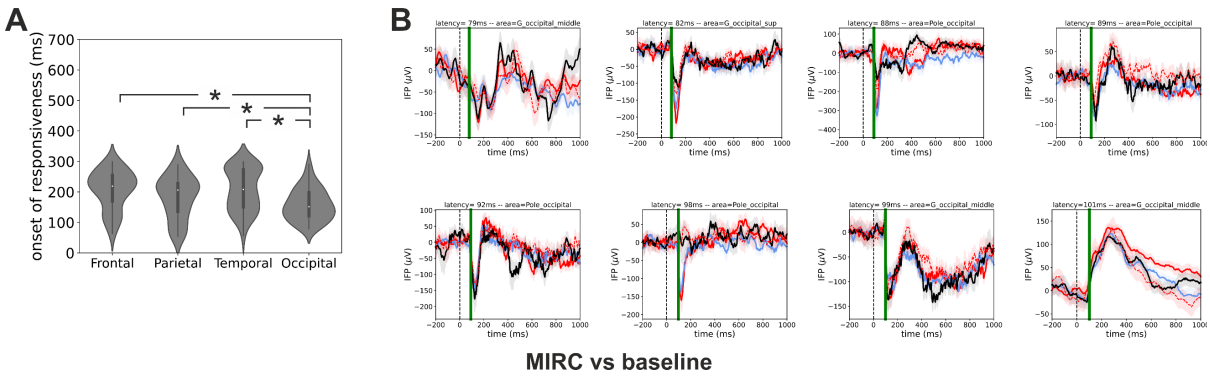

Figure S4 – Visual responses to MIRC stimuli*, Related to* ***Figures 2*** *and* ***3. (A)*** *Distribution of responsivity start times for the MIRC stimuli in the occipital (n=48 electrodes, median=152ms), temporal (n=78, median=208ms), parietal (n=47, median=206ms) and frontal (n=55, median=219ms) lobes. We deemed visually responsive to MIRC stimuli those electrodes whose responses during MIRC trials were statistically different from baseline at a p<0.01 level (Wilcoxon ranksum test) for at least 50 consecutive time points (see Methods). Asterisks signify statistically different responses at the p<0.05 level.* ***(B)*** *Neural responses of the 8 MIRC-responsive electrodes with shortest latency located in the occipital lobe. The response latency and brain area of each electrode are shown in the title.*

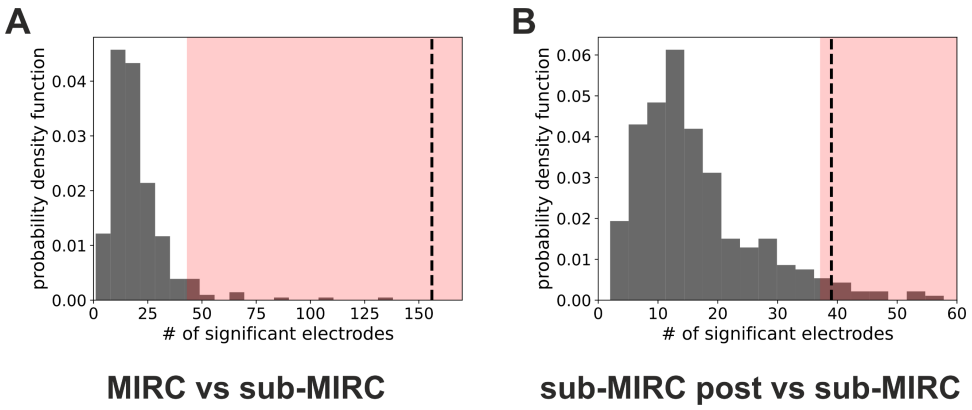

Figure S5 – Distributions of the False Discovery Rate (FDR) of the number of selective electrodes*, Related to* ***Figures 3****,* ***6****, and STAR Methods. The two panels show the distribution of the number of electrodes selective for MIRC versus sub-MIRC (****A****) and sub-MIRC post versus sub-MIRC (****B****) when the condition labels were randomly shuffled 500 times. In each panel, the red shaded area represents the top 5% tail of the distribution, and the vertical dotted line represents the number of selective electrodes found in the corresponding analysis (MIRC vs sub-MIRC: 156 electrodes, and sub-MIRC post vs sub-MIRC: 39 electrodes). In both cases our analyses have FDR < 0.05.*

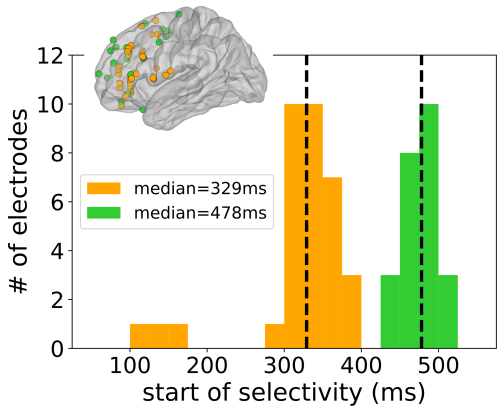

Figure S6 – Histograms of the selectivity start times of responses differentiating between MIRCs and sub-MIRCs in the frontal lobe*, Related to* ***Figure 3****. The distribution was not unimodal (Hartigans's dip test, p<0.005) and it appeared to consist of two components: an "early" and a "late" component, color coded in orange and green, respectively. The legend shows the median of the two distributions and the inset the anatomical locations of the electrodes. The distribution of onset times contains data from 5 participants. At the single-participant level, due to sampling limitations, Hartigan's dip test was significant in only one of our participants.*

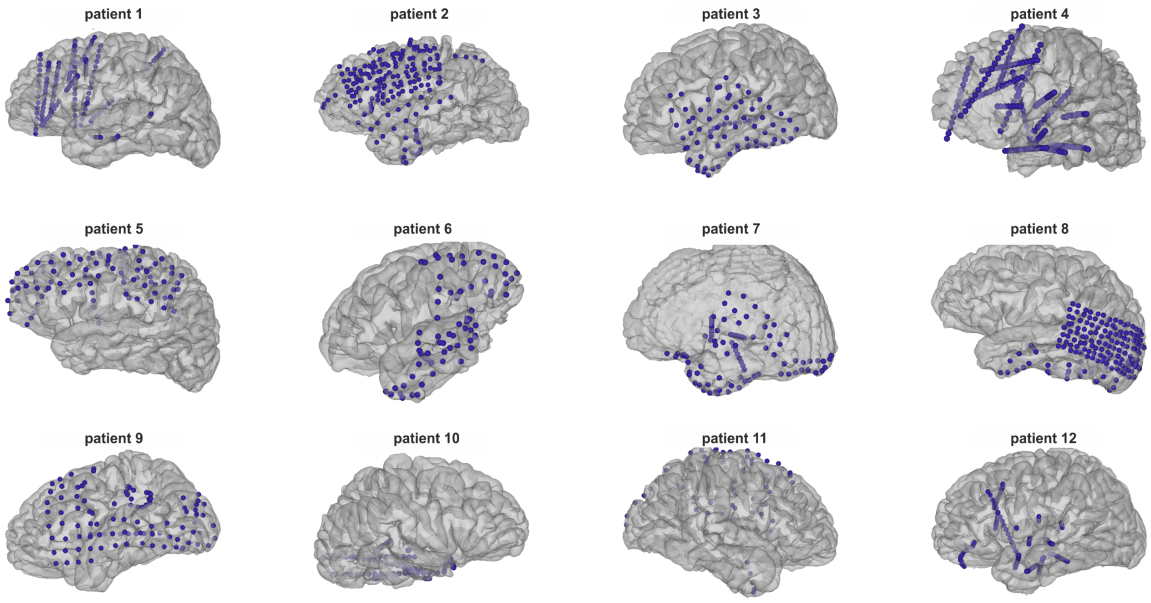

Figure S7 – *Location of electrodes in each of the 12 participants*, *Related to STAR Methods.*

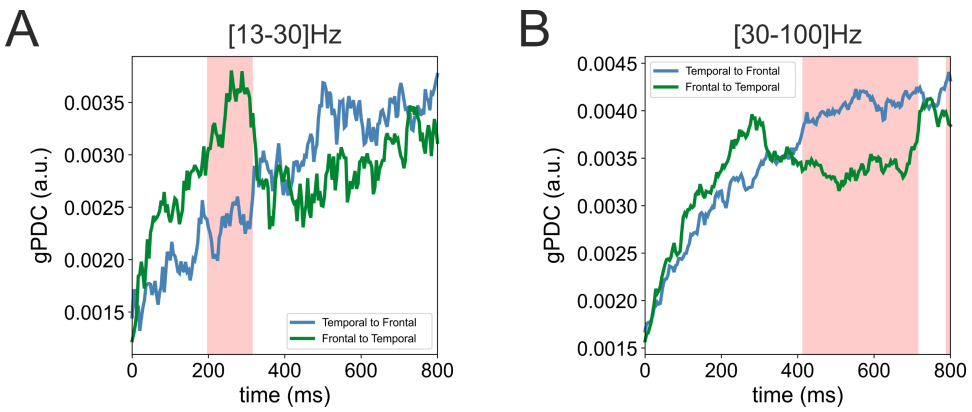

Figure S8 – Results of a frequency-resolved generalized Directed Partial Coherence (gDPC) analysis during the perception of MIRC stimuli*, Related to* ***Figure 4*** *and Discussion. The two panels show the strength, as assessed by generalized Partial Directed Coherence (gDPC, Baccalá et al., 2007), of the temporal to frontal (blue curve) and frontal to temporal (green curve) functional interactions measured in participants (n=6) that had at least 2 responsive electrodes in <u>both</u> the temporal and frontal lobe during the observation of MIRC stimuli. The curves represent the average gPDC obtained from n=3639 pairs of frontal and temporal electrodes respectively. The two panels show the directionality of the functional interactions obtained when the gDPC was integrated in the lower ([13-30]Hz; panel* ***A****) or higher ([30-100]Hz; panel* ***B****) temporal frequency range respectively. Standard errors are shown but they are too small to be visible. Red-shaded areas mark intervals where the interactions in one direction are significantly stronger than in the opposite direction.*